UNIVERSITY
OF OSLO

Master's thesis

Exploring drug sensitivity and Enhertu resistance in breast cancer tissue using *ex vivo* cultures

Emma Tjoflot Degnov

Bioscience: Molecular biology and biochemistry

60 credits

Department of Biosciences

Faculty of Mathematics and Natural Sciences

Autumn 2023

Emma Tjoflot Degnov

Exploring drug sensitivity and Enhertu resistance in breast cancer tissue using *ex vivo* cultures

Supervisors:

Lina Prasmickaite

Solveig Pettersen

Abstract

Ex vivo tumor tissue cultures, such as organoids or explants, hold promise as a drug screening platform for functional precision diagnostics. In this project, we have employed such cultures to investigate functional and molecular properties of breast cancer (BC) tissue with distinct sensitivity to Enhertu, an antibody-drug conjugate (ADC). ADCs are a novel class of cancer therapy, that combines the specificity of monoclonal antibodies with the cytotoxic effects of chemotherapeutic drugs. As of now, three ADCs are approved for the treatment of BC, and two of these (Enhertu and Trodelvy) are tested in this project, using *ex vivo* tissue cultures.

As a model, we used an isogenic pair of BC patient-derived xenografts (PDXs) consisting of the highly sensitive and resistant sublines, HBCx39 and HBCx39ER, respectively. We have shown that the cultured tissue from HBCx39ER was non-responsive to Enhertu, in contrast to the Enhertu-sensitive HBCx39, which validates the responses as seen *in vivo*. Furthermore, the cultured tissue from HBCx39ER was also less sensitive to another ADC, Trodelvy, and to the chemotherapeutic agent, paclitaxel. Thereby, we predicted that HBCx39ER tumors should be less sensitive or resistant to these drugs also *in vivo*, which was later validated by other members of the group. The poor response of HBCx39ER tissue to Enhertu, Trodelvy and paclitaxel suggested that the tissue had developed a multidrug resistance. To investigate the possible mechanisms of resistance, we compared the cultures from both PDXs with respect to: i) expression of the receptors that are targeted by the two ADCs (HER2 and Trop-2) and ii) sensitivity to topoisomerase I inhibition, which is the action of the payloads of both ADCs. We have not observed any difference between the two PDX cultures, suggesting that other resistance mechanisms reason the multidrug resistance. We have detected the presence of the early endosome marker, RAB5, a reported predictive biomarker for HER2-targeted ADC response, in cultures from the Enhertu-sensitive PDX. Unfortunately, the cultures from the Enhertu-resistant PDX were not investigated yet and thus, comparison was not possible. In conclusion, we have demonstrated that tumor tissue cultures are useful *ex vivo* tools for exploration of tumor drug sensitivity and investigation of resistance mechanisms.

Acknowledgements

The work presented in this thesis was carried out at the Department of Tumor Biology, Institute of Cancer Research, Oslo University Hospital, at the Norwegian Radium Hospital in the period June 2022 to November 2023.

First, I would like to express my sincere gratitude to my supervisors, Lina Prasmickaite and Solveig Pettersen, for their invaluable guidance and support throughout this project. Lina, thank you for sharing your extensive knowledge on cancer research, and for always taking the time to discuss and answer my questions. Solveig, thank you for sharing your expertise in the lab, and for always being patient and supportive. I would also like to thank both of you for all the time you have spent thoroughly reading through my thesis and for the help during the writing process. You have been the best supervisors I could ask for.

I would also like to thank Gunhild Mari Mælandsmo for your guidance and feedback, and for allowing me to do a master project in your group. To the members of the Mælandsmo group, thank you for always making me feel welcome, and for your fruitful feedback on my results. Especially, I want to express my gratitude to Geir Frode Øy and Remya Valsala Kumari for providing me with tumor tissue. And to my fellow master student Fatima, it has been a pleasure to share an office with you the last year. Thank you for the support, for all the tea breaks in the office and for the (way too long) lunches.

Lastly, I want to thank my family and friends for their unconditional support and encouragement. It is greatly appreciated.

Oslo, November 2023
Emma Tjoflot Degnov

Abbreviations

ADC = Antibody-Drug Conjugate

AKT = protein kinase B

AUC = Area Under the Curve

ATP = Adenosine Triphosphate

BC = Breast Cancer

BSA = Bovine Serum Albumine

CO_2 = Carbon dioxide

CTG = CellTiter-Glo

DAPI = 4',6-diamidino-2-phenylindole

dH_2O = Distilled water

DMEM = Dulbecco's Modified Eagle's Medium

DNA = Deoxyribonucleic Acid

DNase = Deoxyribonuclease

EEA1 = Early Endosome Antigen 1

EGF = Epidermal Growth Factor

EMT = Epithelial-Mesenchymal Transition

EpCAM = Epithelial Cell Adhesion Molecule

ER = Estrogen Receptor

FITC = Fluorescein isothiocyanate

FDA = US Food and Drug Administration

FGF = Fibroblast Growth Factor

HBCx39 = Human Breast Cancer xenograft 39

HBCx39ER = Human Breast Cancer xenograft 39 Enhertu-Resistant

HER2 = Human Epidermal growth factor Receptor-2

HR = Hormone Receptor

IF = Immunofluorescence

MAPK = Mitogen-Activated Protein Kinase

MDR1 = Multidrug Resistance gene 1

MEK = Mitogen-activated protein kinase kinase

MET = Mesenchymal-Epithelial Transition

mTOR = mammalian Target Of Rapamycin

MTS = 3-(4,5-dimethylthiazol-2-yl)-5-(3-carboxymethoxyphenyl)-2-(4-sulfophenyl)-2H-tetrazolium, inner salt

NADH = Nicotinamide Adenine Dinucleotide

NADPH = Nicotinamide Adenine Dinucleotide Phosphate

OWB = Organoid Washing Buffer

PBS = Phosphate Buffered Saline

PDX = Patient-Derived Xenograft

PDXC = PDX in Culture

PES = Phenazine Ethosulfate

PI = Propidium Iodide

PI3K = Phosphoinositide 3-Kinase

PR = Progesteron Receptor

PTEN = Phosphatase and Tensin homolog

RAB5 = Ras-Associated Binding protein 5

RAF = Rapidly Accelerated Fibrosarcoma kinase

Ras = Rat Sarcoma virus GTPase

RB1 = Retinoblastoma 1

RNA = Ribonucleic Acid

SCID = Severe Combined Immunodeficiency

SMAD4 = SMAD family member 4

TNBC = Triple-Negative Breast Cancer

TP53 = Tumor Protein 53

TRITC = Tetramethylrhodamine

Trop-2 = Trophoblast cell surface antigen 2

Contents

Background

1.1 Cancer

Cancer is a heterogeneous group of diseases, which are all characterized by unregulated cell growth [1]. The cause of cancer is often mutations or genetic alterations (aneuploidy, deletions, inversions, translocations etc.), often leading to abnormal growth and uncontrolled proliferation of cells [2]. This can either be caused by environmental agents or endogenous processes. These genetic changes usually occur in three main types of genes: proto-oncogenes, tumor suppressor genes and DNA repair genes [1]. Proto-oncogenes are normal genes that have the potential to become oncogenic once they are mutated, then called oncogenes. When these genes are mutated, the protein product of the gene has increased production or increased activity, potentially leading to tumor formation. An example of an oncogene is Human Epidermal growth factor Receptor-2 (*HER2*), which is overexpressed in 15-20% of breast cancers [3], and its protein product may be used as a target when treating such tumors [4]. Tumor suppressor genes encode proteins that suppress tumor formation and growth. When these genes are mutated, it can cause a loss of function, which in turn can lead to tumor formation and proliferation [1]. The well-studied tumor suppressor gene, *TP53*, is mutated in over half of cancers, and has a key role in inhibiting carcinogenesis [5]. The protein product of the *TP53* gene, p53, acts as a transcription factor and induces expression of genes that are involved in cell cycle arrest, DNA repair and apoptosis. A loss of function of *TP53* will impair the regulation of the cell cycle, DNA repair and apoptosis, which in turn may lead to cancer progression [6]. Another class of genes that are commonly mutated in cancer are DNA repair genes. DNA repair genes encode proteins that are responsible for repairing damaged DNA. The DNA of most cells in the body is damaged by mutagens on a daily basis. If the cell does not have a functional DNA repair machinery, the damage will not be repaired, which in turn may lead to atypical growth or division of cells [7].

Cancers are grouped based on the organ of origin, e.g. lung cancer or breast cancer. Cancers may also be categorized based on the type of tissue it derives from, e.g. epithelial tissue-derived cancers are called carcinomas, and breast cancer (the focus of this project) belongs to this category.

Generally, tumors can be divided into two broad categories: benign and malignant. Benign tumors grow locally and do not invade adjacent tissue. Malignant tumors are characterized by their ability to leave the primary site and spread to distant sites via the process called metastasis [8].

1.1.1 Metastasis

"Tissue invasion and metastasis" was one of the original hallmarks of cancer suggested by Hanahan and Weinberg in 2000 [9]. Metastatic ability is what differentiates a benign tumor from a malignant tumor. Metastatic cancers represent a major clinical problem.

Cancer can arise in all organs of the body, and the tumor at the origin site is called the primary tumor. From this site, the tumor can release cells (termed circulating tumor cells) that can migrate to other organs in a process called metastasis [10]. Once the circulating tumor cells have arrived at the secondary site, they can pierce through the basement membrane of the organ and invade the tissue, where they form secondary tumors called metastases [11]. The circulating tumor cells can travel via the lymphatic system or in the blood. In order for the tumor cells to be able to migrate out of the primary tumor and be transported through blood/lymph vessels, they must undergo a transition called the epithelial-mesenchymal transition (EMT) [12]. This is a process in which the highly connected epithelial cells of the primary tumor acquire the properties of the mesenchymal cells, i.e. become differentiated, motile and invasive. The mesenchymal-like cells are able to leave the primary tumor, be transported through the blood or lymph system and reach their colonization site where they undergo the reverse process, mesenchymal-epithelial transition (MET). Following this, the secondary tumor is formed [13].

1.2 Breast cancer

Breast cancer (BC) is the most common cancer diagnosis for women, making up for 22% of cancer incidences for women in Norway [14]. The incidence rate of breast cancer has increased drastically over the last decades, partly because patients are diagnosed earlier now than in the last decades [14]. BC is one of the leading causes of cancer deaths in women [15], highlighting the importance of better and more efficient treatment of BC.

The BC carcinoma commonly arises in the lobules and ducts of the mammary glands [16]. The normal human mammary glands are made up of hollow branches and lobes, surrounded by adipose and connective tissue (Figure 1). Each breast consists of 15-20 lobes of glandular epithelial tissue, each lobe branching out into smaller secretory lobules, which leads to a lactiferous duct. The lobes are arranged in a radial manner converging towards the nipple [17].

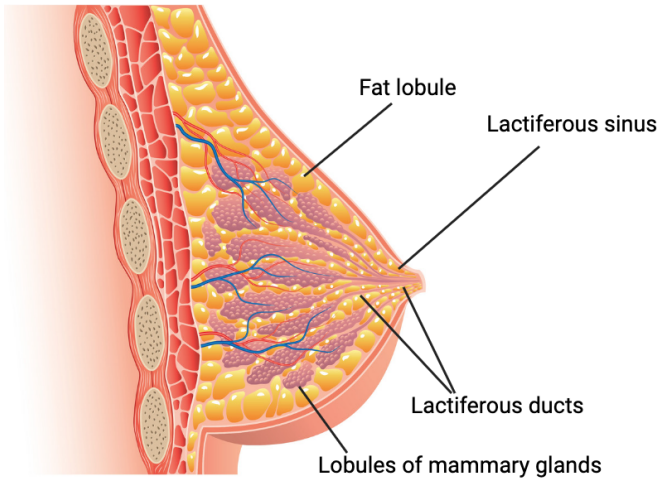

Figure 1: Cross-section of a normal breast anatomy.
Image modified from: https://www.istockphoto.com/vector/breast-anatomy-isolated-on-white-vector-gm536895135-57628950. Image generated in BioRender.

The development of breast cancer extends over a long period of time, starting with genetic alterations in a single epithelial cell in the lobe of the mammary gland. When this cell divides and grows, a primary tumor is formed, and in some cases the cancer may spread to distant organs, forming metastases. The common sites of metastases for BC are lung, bones, brain and liver [18].

1.2.1 Classification of breast cancer

The most common and widely used classification of breast cancers is based on the expression of hormone receptors (HR) on the cancer cells: Estrogen Receptor (ER), Progesterone Receptor (PR) and Human Epidermal growth factor Receptor 2 (HER2). There are four main subtypes of breast cancer: luminal A, luminal B, HER2-positive and triple-negative breast cancer (TNBC) [19]. The prevalence of each subtype is specified in Figure 2.

Luminal A subtype tumors are characterized by expression of ER and/or PR, and by having low expression of the proliferation marker Ki67 (less than 20%). These tumors are slow-growing and the patients have good prognosis, and a higher survival rate [19].

Luminal B subtype tumors are ER-positive, and can be HER2-positive or -negative [20]. Patients with luminal B tumors have worse prognosis than patients with Luminal A tumors.

HER2-positive subtype of tumors are characterized by overexpression of HER2. HER2 is a transmembrane tyrosine kinase that, when activated, provides the cell with proliferative and anti-apoptotic signals, causing tumor development and progression. Overexpression of HER2 has been found to correlate with poor prognosis [21].

TNBC tumors are ER- and PR-negative and lack overexpression of HER2. These tumors are usually highly proliferative and represent the most aggressive subtype, where resistance to treatment and metastases are often observed [22].

1.3 Cancer therapy and drug resistance

1.3.1 Standard treatment for breast cancer

The treatment of BC depends on the tumor subtype and its underlying biology. The HR+ tumors are hormone-sensitive, i.e. their growth is dependent on the binding of hormone to hormone receptors, initiating downstream signaling. Therefore, such tumors can be treated with hormone therapy targeting this axis [24]. There are several main strategies of hormone therapy, either to block production of hormones (like aromatase inhibitors) or to interfere with the signaling via the hormone receptors (like tamoxifen). Hormone therapy can be combined with another targeted drug, like everolimus. Everolimus is a protein kinase inhibitor of the mTOR kinase, one of the

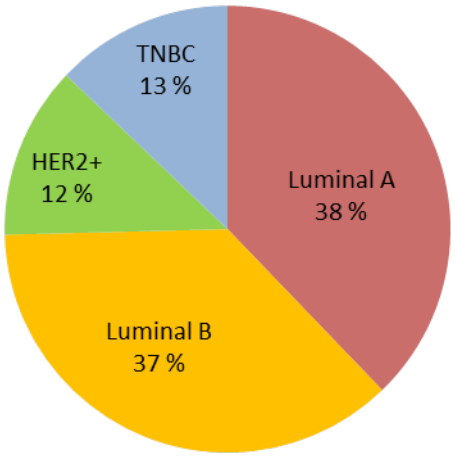

Figure 2: The prevalence of BC subtypes, based on a study including 864 BC patients. Image is modified from Zhang et al. [23].

major components of the oncogenic PI3K/AKT/mTOR signaling pathway [25]. This signaling pathway is often activated in several subtypes of BC, including TNBC [26]. A combination of everolimus and hormone therapy has been shown to significantly improve progression-free survival in HR+ patients [27].

HER2+ tumors are usually treated with HER2-targeted therapies. Anti-HER2 drugs, like the monoclonal antibodies trastuzumab and pertuzumab, work by binding to the extracellular domain of the HER2 receptor, preventing its dimerization and activation of downstream signal-transduction pathways (PI3K and MAPK) [28]. Another class of HER2-targeting drugs is tyrosine kinase inhibitors, like lapatinib and tucatinib. They bind to the intracellular domain of HER2, preventing the kinase activity and thus the downstream signaling [29]. The HER2 signaling pathway is illustrated in Figure 3. Recently a novel treatment option for HER2+ BC patients has entered the clinic. These are antibody-drug conjugates (ADCs) that combines the specificity of anti-HER2 antibodies and the cytotoxic effect of the internalized drug.

For TNBC, due to the lack of drug-targetable receptors, the standard treatment is chemotherapy [30]. Chemotherapy targets DNA, RNA or protein to disrupt the cell cycle, thus it affects rapidly proliferating cancer cells [31]. In Norway, TNBC patients are treated with a combination of two chemotherapy drugs: epirubucin and cyclophosphamide. The anthracyclin, epirubucin, acts by inhibiting the activity of

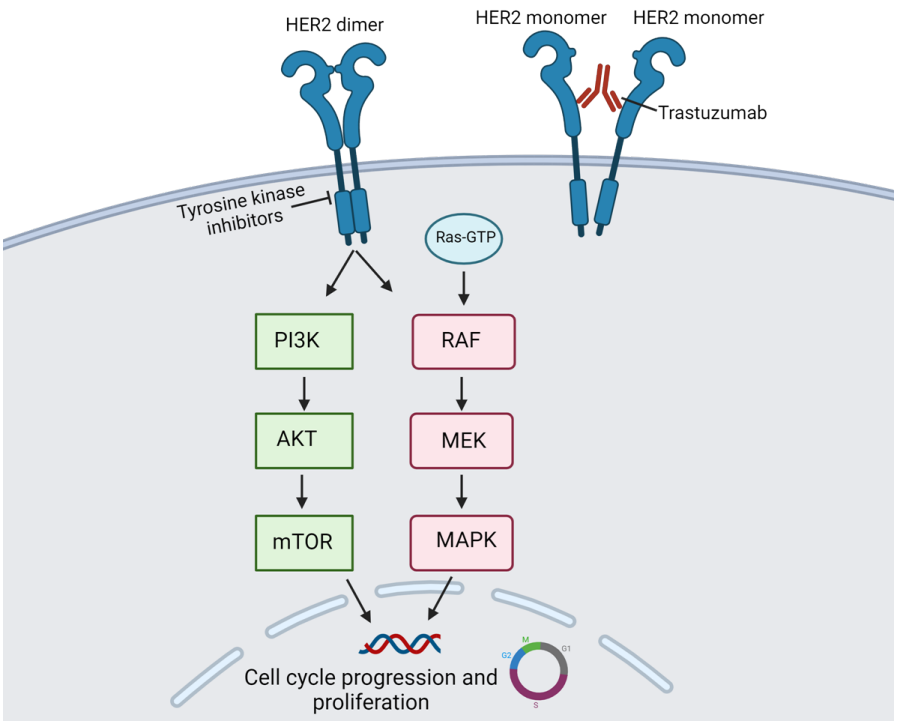

Figure 3: The signaling pathway of HER2. The figure also includes the mechanisms of action of tyrosine kinase inhibitors and trastuzumab. Image generated in BioRender.

topoisomerase II, by intercalating adjacent DNA base pairs [32]. Cyclophosphamide is an alkylating agent which prevents cell division by cross-linking DNA strands and inhibiting DNA synthesis [33]. Following this, the patient is treated with taxanes, e.g. paclitaxel [34]. Paclitaxel blocks the breakdown of microtubules at the end of mitosis, leading to cell-cycle arrest and ultimately cell death [35]. It has been attempted to combine chemotherapy with the mTOR inhibitor everolimus, but no synergistic effect have been observed in the TNBC patients [26].

1.3.2 Antibody-drug conjugates (ADCs)

Clinical application of ADCs in BC

During the last years, a novel class of targeted drugs, antibody-drug conjugates (ADCs), have been under rapid development. Initially, ADCs were developed to improve the treatment of HER2+ BC. Kadcyla (trastuzumab-emtansine) was the first ADC to get approved for the treatment of BC by the US Food and Drug Administration (FDA) in 2013. It was approved for the treatment of metastatic HER2+ BC [36]. In 2019,

Enhertu (trastuzumab-deruxtecan), was approved for the treatment of advanced HER2+ BCs [37]. Trodelvy (sacituzumab-SN-38) was in 2020 the first ADC to receive FDA-approval for metastatic TNBC. Later, also Enhertu received approval from the FDA and the European Medical Agency for advanced metastatic HER2-low TNBC [38]. In Norway, Enhertu was approved in September of 2023, for the treatment of patients with metastatic HER2-low BC, who had previously been treated with chemotherapy [39].

Structure of ADCs

ADCs are created by linking a payload (a cytotoxic drug) to an antibody that recognizes an antigen on the target cell [40], as illustrated in Figure 4. This improves the delivery of the cytotoxic drug.
The payload in ADCs can be divided into two groups: antimicrotubule compounds like emtansine (a constituent of Kadcyla) or DNA damaging agents, like deruxtecan (in Enhertu) or SN-38 (in Trodelvy) [41]. Antimicrotubule compounds can further be divided into two subgroups: maytansinoids or auristatins. Both maytansinoids and auristatins inhibit microtubule polymerization, which causes mitotic arrest and eventually resulting in apoptosis [42], [43].

DNA damaging agents are divided into two subgroups: topoisomerase inhibitors or DNA intercalators. Topoisomerase I is an enzyme located in the nucleus of the cell, that is capable of changing the topology of DNA by inducing a single-strand break in the DNA. This unwinds the supercoiled DNA-molecule, and ultimately the topoisomerase I seals the single-strand break [44]. When this action is inhibited, the DNA will remain supercoiled, thereby inhibiting replication of the DNA, ultimately leading to cell death [45]. DNA intercalators act on the minor groove of DNA, introducing double-strand breaks, which eventually leads to apoptotic cell death [46].

As a targeting moiety in ADCs used for BC treatment, the most often utilized antibodies are the anti-HER2 antibody trastuzumab or its modified versions (like in Kadcyla and Enhertu), or antibodies targeting Trop-2 (like in Trodelvy). Tumor-associated calcium signal transducer 2 (Trop-2) is a transmembrane calcium signal transducer. The expression of Trop-2 on BC cells is associated with cell growth, division and spread of cancer. Overexpression of Trop-2 is associated with poor prognosis [47].

The linker of the ADC can be either cleavable or non-cleavable. The cleavable linkers

can be cut in response to environmental factors such as lysosomal proteases, gluthatione reduction and changes in pH, which releases the cytotoxic payload. The release may occur not only inside the cell, but also extracellularly in the tumor microenvironment [48]. When released, the payload of the ADC can act also on other cancer cells in proximity. These cells may not express the antigen, but they will nevertheless be affected by the cytotoxic drug. This is called a bystander effect [49], which is expected to enhance the anti-cancer efficacy of the ADC [50]. ADCs with non-cleavable linkers do not exhibit the bystander effect.

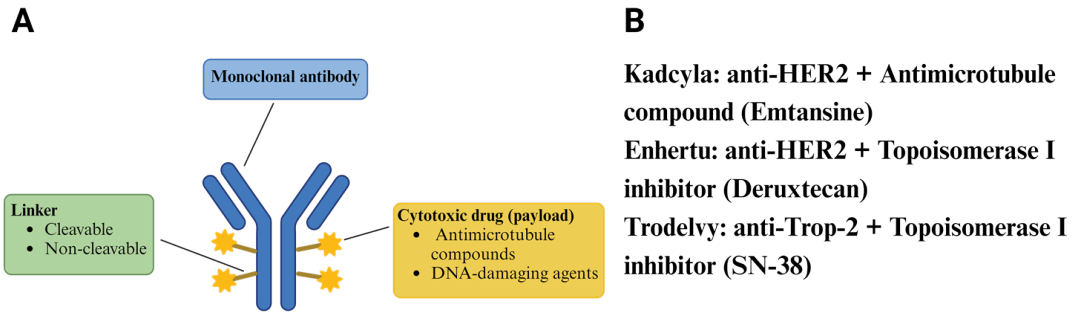

Figure 4: **A:** Schematic representation of an antibody-drug conjugate (ADC). **B:** Overview of the components (antibody + payload) of the ADCs Kadcyla, Enhertu and Trodelvy. Image generated in Biorender.

ADC mechanism of action

The main steps of ADC internalization is illustrated in Figure 5. The antibody of the ADC binds its antigen, and the antigen-ADC complex is internalized via receptor-mediated endocytosis [51]. Internalization results in inward budding of the plasma membrane, forming an early endosome [21]. The early endosome matures into a late endosome, before it fuses to lysosomes. The transport of the antigen-ADC complex in endosomes to lysosomes, is mediated by several proteins and mechanisms. An early endosome protein, RAB5, has been reported to be a predictive biomarker for sensitivity to the ADC, Kadcyla [52]. RAB5 is involved in the delivery of the antigen-ADC complex from the plasma membrane to the early endosome, as well as in endosome fusion [53]. In the lysosome, the cleavable linker may be degraded. After cleavage, the cytotoxic drugs are transported from the lysosomal lumen to the cytosol, and then it is further

transported to the nucleus, where the payload can exert its action. The cytotoxic effects of the payload finally leads to cell death. The liberated cytotoxic drug will have high intracellular concentration and it is membrane permeable, and is therefore capable of exerting bystander effect [21].

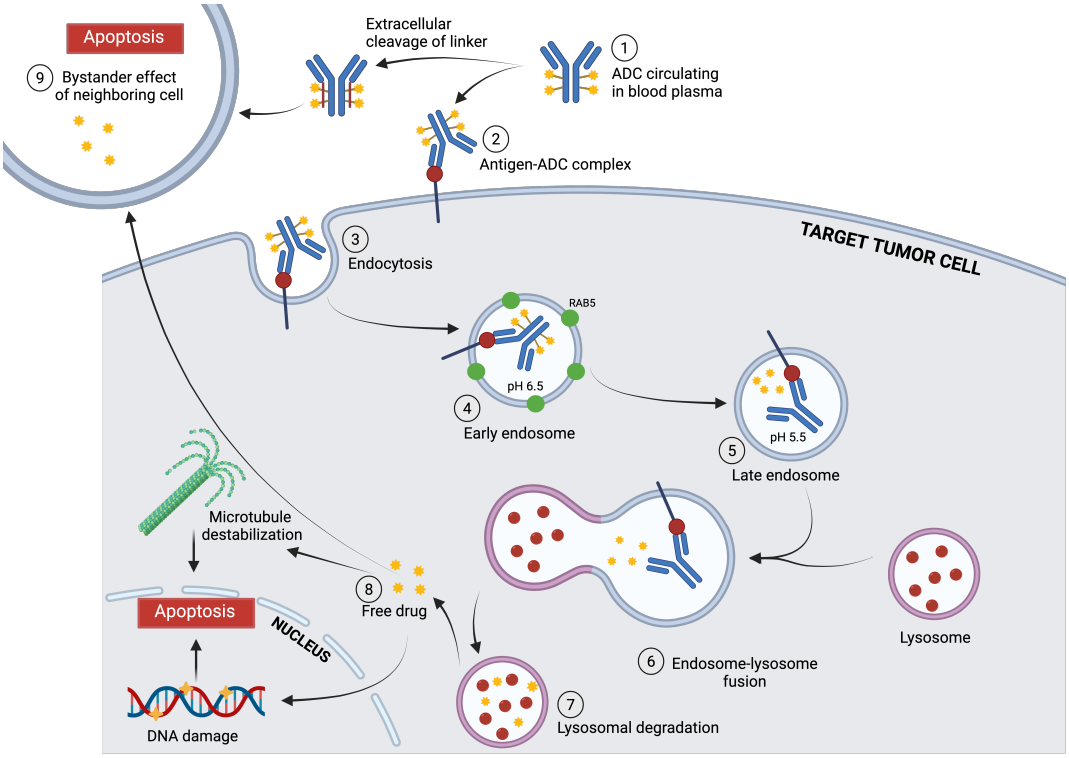

Figure 5: Mechanism of action of ADCs. The antigen-ADC complex is taken up into the cell via endocytosis. The ADC is transported in endosomes, before the endosome fuses with a lysosome, from where the payload of the ADC can be released into the cytosol and nucleus. The payload exerts its cytotoxic effect, killing the target cell. The drug may also affect neighboring cells by the bystander effect. Image generated in BioRender.

TNBC tumors do not overexpress HER2, thus alternative cell surface targets have been researched. Trop-2 is overexpressed in several carcinomas, including all subtypes of BC [54]. The Trop-2-targeting ADC, Trodelvy, was approved for treatment of pretreated metastatic TNBC in 2020 [40]. The antibody Sacituzumab binds to Trop-2 on the surface of the cancer cells. Once Sacituzumab has bound its antigen, the ADC is internalized via receptor-mediated endocytosis [55]. The antigen-ADC complex is transported into the nucleus, where SN-38 binds topoisomerase I-DNA complexes, inhibiting the activity of topoisomerase I and preventing the DNA from uncoiling. This leads to single-strand breaks, which in turn triggers apoptotic cell death. Additionally, because of the cleavable

linker, SN-38 may be released both intracellularly and in the tumor microenvironment, exerting a bystander effect [55].

1.3.3 Drug resistance

A big challenge of long-term use of chemotherapy and targeted therapy is drug resistance [1]. The resistance may be present before the start of cancer treatment (intrinsic resistance) or it can be acquired during treatment (acquired resistance). Tumors are heterogenous and may contain cell subpopulations (e.g. with distinct mutational profiles) that respond differently to the same drug [56]. The positioning of the cells within the tumor also affects their exposure to the treatment. The cells in the core of the tumor may have limited blood supply, and are therefore not exposed to the drugs in the same degree as the cells on the surface of the tumor. This also depends on the size of the tumor.

There are several mechanisms a cancer cell can utilize to achieve drug resistance. Some of them are illustrated in Figure 6. The cells may increase the efflux of the drug, or decrease the influx so that the intracellular concentration of the drug is reduced [1]. In order to increase the efflux of drugs, the cell may utilize transmembrane transporters that usually are involved in the movement of nutrients and other molecules across the cell membrane. The multi-drug resistance gene (*MDR1*) encodes a P-glycoprotein that can bind several chemotherapeutic drugs. Once the drug is bound to the transporter, ATP is hydrolyzed, causing a conformational change within the transporter and the drug is released out of the cell [57]. The cell may also alter the metabolism of the drugs, making them inactive.
Cancer cells can also increase the drug target molecules inside the cell by gene amplification. In the case of DNA-targeting drugs, the cell may increase the cellular DNA repair processes [1].
Furthermore, modifications in the pro- and anti-apoptotic balance is known to contribute to drug resistance. Inactivation of the p53 pathway, a strong inducer of apoptosis, causes resistance to pro-apoptotic drugs [58].

For example, two main mechanisms of resistance to paclitaxel is the expression of the *MDR1* gene and alterations in its cellular target, tubulin [59]. Due to increased levels of the multidrug efflux pump, P-glycoprotein, paclitaxel is rapidly pumped out of the cancer cells [60]. Alterations in tubulin structure and expression levels of regulatory

proteins can reduce inhibitory effect of paclitaxel on microtubules [59].

Mechanisms of resistance to targeted therapy:
Several acquired mechanisms of resistance have been reported for targeted therapies. These include the loss of expression of the cellular target, mutations downstream of the target and the activation of additional cell proliferation mechanisms [61].

Mechanisms of resistance to ADCs:
Several mechanisms of resistance to ADCs have been reported [21]. In the case of HER2-targeted ADCs, it can include similar mechanisms as in trastuzumab resistance, i.e. loss of expression or expression of truncated forms of HER2 receptors have been reported as mechanisms of resistance to trastuzumab [62]. Additionally, alterations in proteins involved in downstream signaling pathways may be associated with resistance. For example, the loss or decreased levels of PTEN have been related to resistance to trastuzumab. This causes the constitutive activation of the PI3K/AKT pathway (downstream from HER2), leading to resistance of HER2-targeted therapies [63].
Another possible mechanism of resistance is alterations in the ADC internalization pathway. This could happen via: i) silencing of a protein involved in the endocytosis of the antigen-ADC complex, ii) limiting the ADCs arrival to lysosomes or iii) alterations in the lysosomes themselves (e.g. altered pH, reduced activity of lysosomal enzymes or inhibition of the transport of drugs from the lysosome lumen to the cytosol) [21]. Finally, resistance to ADCs might be reasoned by similar mechanisms as reported for other types of drugs, e.g. the increased expression of drug efflux pumps [64].

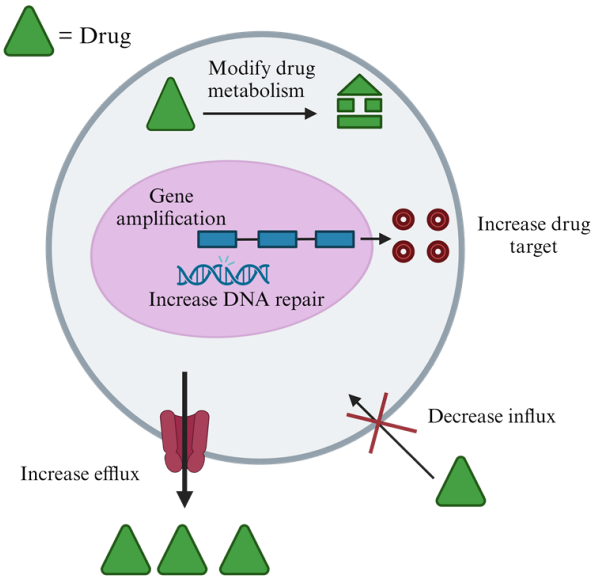

Figure 6: Mechanisms of drug resistance. The cancer cell may utilize different mechanisms in order to achieve drug resistance, including: modification of drug metabolism, gene amplification, increase DNA repair, increase drug target, increase efflux of drug molecules and decrease influx of drugs. Image generated in BioRender.

1.4 Personalized therapy and functional precision diagnostics

Personalized therapy recognizes the heterogeneity of each cancer, and aims to tailor the treatment to each patient based on the characteristics of the individual tumor. Such characteristics are usually understood as genetic abnormalities (like specific mutations, amplifications or gene fusions) that could be exploited as predictive or prognostic biomarkers, helping to select the right treatment for the individual patient [65]. As an example, HER2 overexpression is recognized as a strong predictive biomarker of response to HER2-targeting therapies [52]. Even though a tumor might harbor specific genomic aberrations, it still might not respond to the predicted treatment [66]. Furthermore, some tumors do not harbor any targetable aberrations. In such cases, functional precision diagnostics might be highly useful. Functional precision diagnostics is an emerging area that is aimed to guide personalized treatment based on the functional properties of the tumor, such as its response to drugs [67]. Thereby, one can identify the drugs that the tumor tissue is sensitive to. Functional studies, like screening of drug sensitivity, require

maintenance of viable tumor tissue outside the host. This can be assured through the respective preclinical models.

1.4.1 Preclinical tumor tissue models for functional studies

Patient-derived xenografts (PDXs) are models where tissue from a patient's tumor is implanted into an immunocomprised mouse, where it is allowed to form a tumor. PDXs recapitulate the characteristics of the patient's tumor [68]. Since PDXs can be serially passaged, they provide infinite access to the tumor tissue and can be used for evaluation of its sensitivity to treatment *in vivo*. PDXs have long been considered the best models for such purpose [69]. However, their use is limited due to low throughput and ethical issues [70]. Cultures of patient-derived organoids/explants have become attractive alternatives for drug sensitivity screening *ex vivo*. Patient-derived organoids/explants are models where tumor tissue is collected either directly from a patient or from PDX grown in a research animal. The tumor tissue is then dissociated and a short-term culture of tissue fragments is produced.

Cancer cell lines and PDX models have contributed greatly in BC research. However, the development of cancer cell lines and PDXs from patient material is time-consuming and inefficient, making it nearly impossible for these models to contribute to individualized therapy [71]. On the contrary, short-term cultures of organoids/explants can be used to efficiently perform drug sensitivity screens and molecular analyses on patient tumor tissue, allowing for their use in functional precision diagnostics [71].

For both normal and cancerous breast tissue, it has been hard to create a method for the establishment of organoids. The application of BC organoids/explants in functional precision medicine is not fully established, but several recent studies demonstrate that it is feasible [72]. In [73], they used functional precision diagnostics to uncover two promising treatment candidates for a TNBC patient. This resulted in complete response for the individual and a progression-free survival period which was more than three times longer than for previous treatments. A clinical trial using genomics to predict promising therapies for patients with metastatic cancer, shows that high-throughput genomics could improve the treatment outcomes of patients with advanced cancers [66]. They report that tumor sequencing improves outcome of 33% of patients with advanced cancers, where several of these were BC patients. These results suggests that functional precision diagnostics using BC organoids/explants is feasible and can give beneficial

results when performed in real time, in collaboration with the clinic [73].

Tumor tissue directly from a patient is precious material and is rarely available for testing of early-stage experimental drugs or for mechanistic studies. For such studies, PDX-derived cultures (organoids/explants) are attractive alternatives. Recently, our group has developed a method for PDX tissue processing and culturing for functional studies *ex vivo*. By using an isogenic pair of chemosensitive and chemoresistant PDXs (MAS98.12 and MAS98.12PR), it has been demonstrated that the respective PDX cultures (PDXCs) recapitulates the sensitivity difference seen *in vivo* [74]. This study put the basis for use of the PDXC platform for evaluation of tissue sensitivity to novel treatment options, like ADCs, as used in this project.

1.4.2 PDX models with distinct sensitivity to Enhertu

Recently, our group has developed an isogenic pair of Enhertu-sensitive and -resistant TNBC PDXs, called HBCx39 and HBCx39ER, respectively. HBCx39 PDX has been treated with different concentrations of the HER2-targeting ADC, Enhertu. As shown in Figure 7A, all treated tumors were highly sensitive to the treatment, inducing initial tumor shrinkage. However, majority of the tumors (100%, 80% and 70% in the 2,5 mg/kg, 10 mg/kg and 25 mg/kg groups, respectively) re-grew with time (Figure 7B). The tissue from the relapsed pre-treated (with 10 mg/kg and 25 mg/kg) tumors was passaged into new animals and exposed to the same treatment. None of the tumors were sensitive to the Enhertu treatment, and continued growing like the non-treated controls (Figure 7C). Thereby, the Enhertu-resistant subline of the HBCx39 PDX was established, named HBCx39ER.

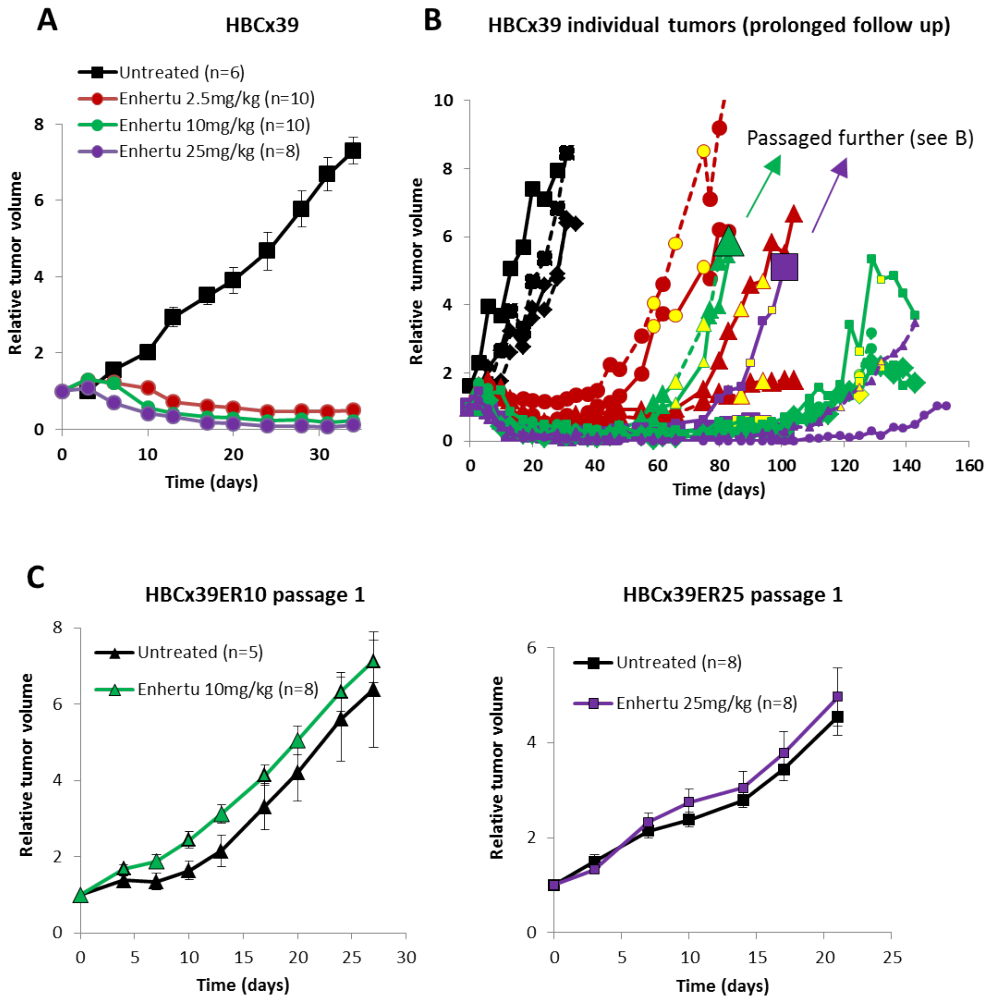

Figure 7: Establishment of the Enhertu-resistant PDX variants HBCx39ER10 and HBCx39ER25. **A:** HBCx39 PDX was treated with the indicated concentrations of Enhertu applied intravenously on days 0, 6, 13 and 20. Tumor growth is presented as tumor volume relative to the volume on the day of the start of the treatment (day 0). **B:** Indicates the growth of individual tumors upon prolonged follow up. The relapsed tumors were treated repeatedly (indicated by the yellow symbols). Two of the relapsed tumors (from the 10 mg/kg and 25 mg/kg groups; indicated by the arrows) were passaged further as HBCx39ER10 and HBCx39ER25 PDX (see C). **C:** The growth of the passaged tumors (p.1) when untreated or treated with the indicated concentrations of Enhertu. *In vivo* experiments were performed by: Geir Frode Øy. Figures were provided by: Lina Prasmickaite.

Aim of study

Recently, our group has developed a method for culturing partially-dissociated tumor tissue from PDX, called PDXC [74]. This method allows for *ex vivo* testing of tissue sensitivity to drugs and holds promise for application of patient biopsies with the purpose of functional precision diagnostics.

The aim of this project was to apply the PDXC method to explore the drug sensitivity of the tissue from TNBC PDXs, HBCx39 and its Enhertu-resistant derivative, HBCx39ER. Furthermore, to explore possible mechanisms of Enhertu-resistance.

The specific aims of this project were to utilize PDXCs to:

- Validate that Enhertu sensitivity/resistance seen *in vivo* can be recapitulated in respective cultures *ex vivo*.
- Compare responsiveness of Enhertu-sensitive and -resistant tissue to another ADC, Trodelvy, as well as to other selected anticancer drugs.
- Explore possible ADC-resistance mechanisms by immunofluorescence-based analyses of PDXCs.

Materials and methods

3.1 Materials

3.1.1 Cell line

In this project, the commercially available cell line MDA-MB468 was used. MDA-MB468 is a human breast adenocarcinoma cell line that was isolated from pleural effusion of the mammary gland from a 51-year old female patient with metastatic breast cancer [75] (Table 3.1). MDA-MB468 is a TNBC cell line. The cells are adherent and have epithelial morphology. The cell line was made refractory to paclitaxel by continuous treatment with 3 nM paclitaxel over a 4 month period (performed by other members of the group). The refractory cells are referred to as MDA-MB468PR, and cells that are sensitive to paclitaxel are referred to as MDA-MB468PS.

Table 3.1: Cell line table: characteristics and donor information [75].

Cell line	**Age/Gender**	**Metastasis**	**Mutations**
MDA-MB468	51 (F)	Yes (pleural effusion)	PTEN RB1 SMAD4 TP53

3.1.2 PDX models

In this project, the tissue from two *TP53*-mutated TNBC PDX models was used. The two PDXs are MAS98.12 (both paclitaxel-sensitive and paclitaxel-resistant variants, MAS98.12PS and MAS98.12PR, respectively) and HBCx39 (both Enhertu-sensitive and Enhertu-resistant, HBCx39 and HBCx39ER, respectively). The two models are very different regarding tissue properties and also survival-time in culture *ex vivo*. The MAS98.12 PDX was established here at the Institute of Cancer Research, Norwegian Radium Hospital [68]. MAS98.12 was developed by transplanting a human primary breast tumor into mice with severe combined immunodeficiency (SCID). The primary tumor was obtained from a patient that had received no treatment prior to the surgery. Further, the primary tumor was implanted subcutaneously into SCID mice. Molecular analyses of the xenograft was performed after the tumor had been passaged 10 times. The xenograft tumor maintained the same morphological and genetic characteristics as the original tumor [68]. The paclitaxel-resistant variant was established from a mouse bearing the MAS98.12 tumor that was treated with 15 mg/kg paclitaxel twice per week for three weeks [74].

HBCx39 PDX was established at the Institute Curie (Paris, France). The xenografts were maintained here at the Institute of Cancer Research, Norwegian Radium Hospital by serial passaging, where pieces of the parental tumor were implanted into the thoracic mammary glands of mice [74]. Enhertu-resistance was established by treatment with 10 or 25 mg/kg Enhertu to a mouse bearing the HBCx39 tumor (as shown in Figure 7). The PDXs were dissociated and cultured in a medium referred to as Reduced Clevers+, modified from [71]. The contents are described in Table 3.2.

Table 3.2: PDXC medium (Reduced Clevers+).

Medium components	**Supplier**	**Catalogue number**	**Final concentration**
Advanced DMEM/F12	Invitrogen	12634-010	1x
GlutaMax 100x	Invitrogen	12634-034	1x
Hepes	Invitrogen	15630-056	10 mM
Penicillin/Streptomycin	Invitrogen	15140-122	100 U/ml
R-Spondin-3	Peptrotech	120-44	250 ng/ml
Neuregulin 1	Peprotech	100-03	5 nM
FGF 7	Peprotech	100-19	5 ng/ml
FGF 10	Peprotech	100-26	20 ng/ml
EGF	Peprotech	AF-100-15	5 ng/ml
Noggin	Peprotech	120-10C	100 ng/ml
Y-27632	Abmole	Y-27632	10 µM
B27 supplement	Gibco	17504-44	1x
N-Acetylcysteine	Sigma	A9165-5g	1.25 mM
Nicotinamide	Sigma	N0636	5 mM
Nutlin-3	Cayman	10004372	10 µM

After 10 days of treatment, the PDX cultures were fixed and stained with immunofluorescent dyes. The antibodies and stains used are described in Table 3.3.

Table 3.3: Immunofluorescence. Antibodies/dyes used for immunofluorescent staining.

Primary antibodies/dyes	**Supplier**	**Catalogue number**	**Dilution**
Anti-EpCam	Novusbio	NBP2-44644	1:50
Anti-panCK	AbCam	Ab86734	1:100
Anti-Ki67	Invitrogen	PA5-114437	1:500
Anti-RAB5	Invitrogen	PA5-29022	1:100
Anti-Trop-2	AbCam	Ab214488	1:100
Anti-HER2	Cell Signaling	2242S	1:100
Hoechst	Invitrogen	H3570	1:6000
DAPI	Sigma-Aldrich	D9542	1:2500
Secondary antibodies			
Donkey anti-rabbit Alexa 555	Invitrogen	A32789	1:400
Goat anti-mouse IgG1 Alexa 488	Invitrogen	21141	1:400

Upon immunofluorescent staining, blocking was performed using Organoid Washing Buffer (OWB) (described in Table 3.4). This buffer was also used to dilute the antibodies [76].

Table 3.4: Components of OWB [76].

Components	**Supplier**	**Catalogue number**	**Concentration**
PBS	Sigma-Aldrich	D8537	
BSA	Sigma-Aldrich	10735086001	0,1%
Triton X-100	Sigma-Aldrich	T9284	0,02%

As a last step to immunofluorescent staining, a fructose-glycerol clearing solution was added (described in Table 3.5).

Table 3.5: Components of Clearing solution [76].

Components	Supplier	Catalogue number	Concentration
dH_2O			
Glycerol 87%	Merck	1.04094.0500	60% (vol/vol)
Fructose	Sigma-Aldrich	F0127	2,5 M

3.2 Methods

3.2.1 Cell culturing

Cell culturing

MDA-MB468PS and MDA-MB468PR were grown as a cell monolayer in tissue-culture flasks in Dulbecco's Modified Eagle's Medium (DMEM) (Sigma-Aldrich, St.Louis, MO, USA) supplemented with 1% Glutamax and 10% serum. The cells were passaged twice a week.

4000 cells per well were seeded in a clear 96-well plate for Incucyte S3-monitoring and MTS, and in a white 96-well plate for CTG. The following day, the cells were treated with paclitaxel at different concentrations (3 nM, 4 nM, 5 nM and 6 nM) and incubated for 4 days.

Cell counting

Automatic counting:
To determine the cell concentration, 10 µl of the cell suspension was mixed with 10 µl trypan blue. 10 µl of the mix was applied to a counting chamber, and inserted into a cell counting instrument (Countess II, Invitrogen). Trypan blue is a dye that stains dead cells which can give the percentage of viable cells of the total cell count.

Manual counting:
For counting manually, 10 µl of cell suspension was applied to a Bürker cell counting slide. The number of cells in 3 A-squares were counted, and the average of these were calculated. The concentration of cells per ml was calculated by multiplying the average cell count per square with the dilution factor and 10^4 (described in Figure 8).

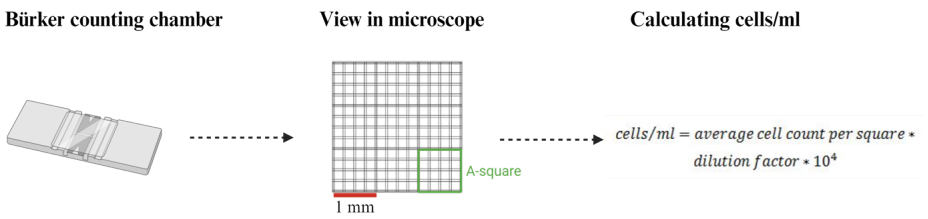

Figure 8: Manual cell counting using a Bürker counting chamber. An A-square is indicated in green. Viable cells are counted, and the average count per A-square is multiplied with the dilution factor and 10^4.

3.2.2 Analysis of cell growth

The growth/proliferation of the cells were measured by using the Incucyte S3 (Sartorius, Gottingen, Germany). The Live-Cell analysis system was used to monitor the cell growth over a 4-day period. Images were captured every 4 hours.

3.2.3 Cell viability assays

MTS

The CellTiter96® AQueous One Solution Reagent (Promega, Madison, WI, USA) contains an MTS tetrazolium compound in addition to an electron coupling reagent phenazine ethosulfate (PES). When adding the reagent, the medium turns brown over time. This is because the MTS compound is converted to formazan by dehydrogenases in metabolically active cells, producing NADPH or NADH. The quantity of formazan product is measured by absorbance at 490 nm, and is directly proportional to the amount of living cells in the culture [77]. The MTS reagent was added to the wells with a dilution ratio of 1:10, following an incubation for 3 hours at 37°C and 5% CO_2. The absorbance was recorded by the Victor X3 plate reader (PerkinElmer, Waltham, MA, USA).

CellTiter-Glo®

CellTiter-Glo® 2.0 Reagent Cell Viability Assay (Promega, Madison, WI, USA) (CTG) is another assay used to determine the number of viable cells in culture. The assay is based on the quantity of ATP present. ATP is used as a marker of metabolically active cells.

When adding the reagent, the cells are lysed, which in turn leads to a luciferase reaction. Luciferin reacts with oxygen and ATP from the lysed cells, which leads to luminescent signals according to the amount of ATP present. The signal is directly proportional with the amount of viable cells in culture [78]. The CTG reagent was added to the wells in a 1:4 dilution, followed by shaking for 2 minutes on an orbital shaker to induce cell lysis. The plate was left at room temperature for 10 minutes to stabilize the luminescent signal, before the signal was recorded by the Victor X3 plate reader (PerkinElmer, Waltham, MA, USA).

3.2.4 PDX tissue cultures (PDXC)

Fresh tumor-tissue or freshly thawed tumor-tissue was chopped with a scalpel in phosphate-buffered saline (PBS)/1% bovine serum albumin (BSA) (both Sigma-Aldrich, St.Louis, MO, USA). The minced tissue was digested with 2 mg/ml collagenase IV and 100 µg/ml DNase (Sigma-Aldrich) diluted in Advanced DMEM F12 medium supplemented with Glutamax, Hepes and Penicilin/Streptomycin, at 37℃ with rotation for approximately 50 minutes. The gentleMACS was used for additional digestion of the tissue (Miltenyi Biotec, Germany), using the m_impTumor_03 setting. This step was left out when handling the MAS98.12 tumors, as these have a softer structure than the HBCx39 tumors. This is an example of the need to optimize this protocol depending on which tissue is being dissociated. The tissue suspension was diluted with PBS/1% BSA and centrifuged for 4 minutes at 18 g. The pellet was resuspended with PBS/1%BSA, then centrifuged at 32 g for 4 minutes. This step was repeated with a speed of 200 g. The final pellet was resuspended with reduced Clevers+ medium (products and concentrations described in Table 3.2). The tissue suspension was seeded out in a 24-well plate, coated with anti-adhesive rinsing solution (Stemcell, Canada, cat number: 07010) in advance. Reduced Clevers+ medium was added to the wells and the fragments were incubated overnight. The suspension was then filtered through a 200 µm cell strainer in order to separate the fragments based on size, and the collected fragments were allowed to sediment for 5-10 minutes. Sedimentation allows the larger fragments to sink to the bottom of the tube, while the supernatant contains single cells. Following sedimentation, the pellet was resuspended in reduced Clevers+ medium, seeded out and further incubated overnight. Another filtration step followed, now filtrating with a 100 µm filter. The collected fragments sedimented for 5-10 minutes, and the resulting pellet was used

to establish PDXCs [74].

Matrigel® Matrix, Growth Factor Reduced (Corning, New York, USA) was added to the fragment suspension to a concentration of 33%. A 10 µl droplet of the fragment-Matrigel mix was seeded in each well of a 48-well plate. Fragments were counted manually using a light microscope, with a concentration of 50-60 fragments per droplet. The droplets were allowed to polymerize for 30 minutes at 37℃ , following addition of reduced Clevers+ medium and incubation overnight at 37℃ . The next day, the PDXCs were treated with various drugs diluted in reduced Clevers+ medium. Half of the medium was replaced every 3-4 days, in addition to re-treatment with the drugs [74].

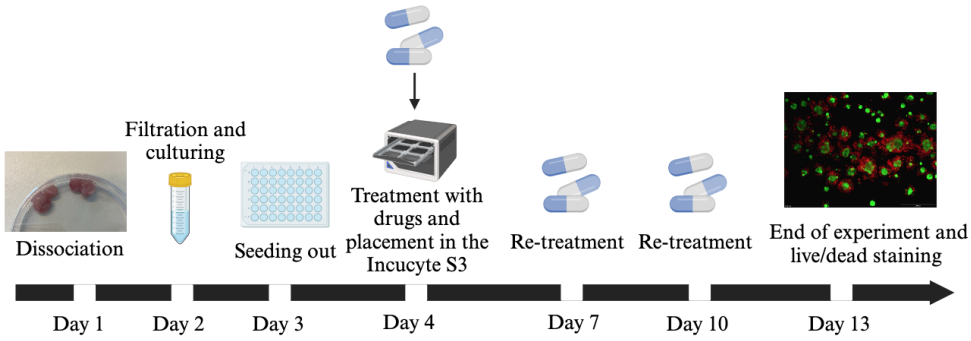

Figure 9: Workflow for the HBCx39 PDXC method from fresh tumor tissue. The method takes approximately 13 days from start to finish, including the dissociation of tumor tissue, filtration and culturing, seeding out in Matrigel, drug application, and the experiment ends with live/dead staining.

Drug sensitivity assessment screen

A drug screen was set up in 48-well plates. The drugs were added at 3x concentration, as 2/3 of the reduced Clevers+ medium was added to the tissue-Matrigel droplets in advance. Three parallels of each concentration was set up, including 3 wells with untreated controls. The concentrations of the different drugs were decided based on previous *ex vivo* and *in vivo* experiments. For the ADCs, Enhertu and Trodelvy, dose response experiments were performed, as the appropriate doses had not yet been decided for *ex vivo* experiments. Irinotecan had not been tested in the PDXC method before, only in cell line studies. The same concentration of irinotecan as used in the cell line studies, were used in the PDXC drug screen (0,25 µM, 1 µM and 2 µM). These concentrations

were increased after observing the dose response in the first PDXC experiment, and in the following PDXC experiments the concentrations used were 0,5 µM, 2µM and 5 µM.

Analysis of growth

The growth, morphology and death of the aggregates were analyzed in real-time by the Incucyte S3, using the organoid analysis software module (Sartorius, Gottingen, Germany). The Incucyte instrument uses phase contrast and brightfield microscopy, and allows for live imaging of the samples. Directly after applying the drugs, the plates were placed in the Incucyte. Images were captured every 6 hours for 10 days. The Incucyte instrument is placed inside an incubator holding 37℃ and containing 5% CO_2.

Area under the curve

The growth curves generated from the data obtained from the Incucyte S3 were used to calculate the area under the curve (AUC), a number that represents the relative growth of the fragments. This measurement is used because it reflects the entire fragment growth curve as a single number, allowing for easier comparison between groups [79]. AUC was calculated using the GraphPad Prism software.

Live/dead staining

Both the untreated and treated PDXCs were stained with 1 µM Calcein-AM (Sigma-Aldrich) for 45 minutes at 37℃ . Following this, they were stained with 300 nM Propidium Iodide (PI) (Invitrogen, Waltham, MA, USA) for 15 minutes at 37℃ . Calcein-AM stains live cells (green) and PI stains dead cells (red). To visualize this, images were captured of the stained cultures by the Olympus IX81 microscope with 4x and 10x objective and filters 488/527 FITC (for Calcein-AM) and 540/590 TRITC (for PI) (Olympus, Tokyo, Japan). To cover the whole area of the droplet, three pictures were taken in each well.

PI is used for identifying dead cells. It is a membrane-impermeant solution, and thus cannot pass through the plasma membrane of viable cells. PI binds DNA and RNA and once the dye has bound the nucleic acids, its fluorescence is enhanced [80].

Calcein-AM is used for identifying live cells. It is a membrane-permeant solution, making it able to penetrate the plasma membrane of viable cells. Calcein-AM has high hydrophobicity, and this characteristic is what makes it possible for it to pass through the membrane. Before permeating the plasma membrane, Calcein-AM is non-fluorescent. Once in the cytoplasm of the cell, Calcein-AM is hydrolyzed, converting it into the green fluorescent Calcein. Compared to Calcein-AM, Calcein has low hydrophobicity, inhibiting it from passing through the plasma membrane and exiting the cell [81].

Quantifying live/dead staining

Live/dead images were quantified using the image processing-software Fiji/ImageJ. The software was used to measure the area of the PI- and Calcein-signals in the pictures. The ratio of live cells in the images were calculated by dividing the Calcein-area with the total signal (PI + Calcein).

Cell viability assay

CellTiter-Glo® 3D (CTG) (Promega, Madison, WI, USA) (specially designed for 3D cultures) was used to determine the amount of viable cells in the PDXCs [82]. The PDXCs were prepared in white 96-well plates with a clear bottom (Corning, New York, NY, USA) and treated for 10 days. The reagent was added to the wells in a 1:4 ratio, followed by shaking on an orbital shaker. The luminescence was recorded by the Victor X3 plate reader (PerkinElmer, Waltham, MA, USA) after 30, 45 and 60 minutes to determine the timepoint where the signal was at maximum.

3.2.5 Immunofluorescent staining and confocal microscopy

For IF, the fragments are seeded in 8-well chamber slides with a glass bottom (Ibidi, Gräfelfing, Germany). The fragments are treated at day 0, following re-treatment every 3-4 days. They are incubated at 37°C for 10 days. Following, the fragments were fixed with 4% paraform aldehyde (PFA) (Chemi-Teknik) for 20 minutes in room temperature. 0,2% Triton X-100 was added to the cultures and left for incubation for 1 hour, in order to permeabilize the cells. The cells are permeabilized for the antibodies to be able to pass through the cell membrane. Following this, blocking was performed using OWB (Table 3.4) for 1 hour at room temperature. Blocking is performed to minimize the background signals from non-specific antigens, resulting in the binding of only the

targeted antigens. Primary antibodies were diluted in OWB before addition to the wells, and incubated overnight at 4℃ with slight shaking. Appropriate antibody incubation times are crucial when immunostaining 3D-structures, because the antibodies may have to penetrate several layers of cells [76]. Longer incubation time is needed compared to staining cells in 2D. Following incubation overnight, the samples were washed with OWB for 3*10 minutes. Then they were incubated with secondary antibodies and DAPI (Table 3.3) diluted in OWB, overnight at 4 ℃ with slight shaking. The samples were again washed in OWB for 3*10 minutes. As a last step, a fructose-glycerol clearing solution (Table 3.5) was added to the wells [76]. Imaging was performed using the Nikon SoRa spinning disk confocal microscope (Nikon, New York, USA) and the ZEISS LSM 710 confocal microscope (Carl Zeiss, Jena, Germany) using the 20x and 40x air objectives.

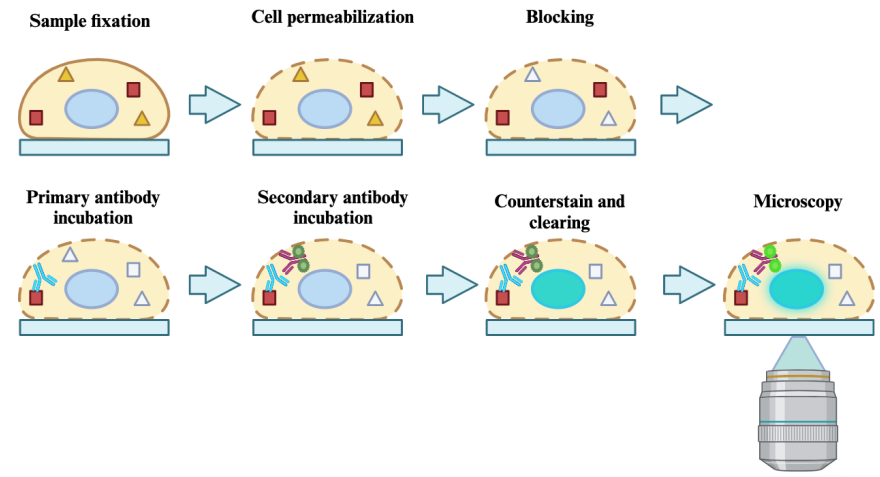

Figure 10: Workflow of immunofluorescent staining. Image was inspired by Ibidi, and created in BioRender.

Results

4.1 Assays for exploring treatment sensitivity of preclinical models

4.1.1 *In vitro* preclinical model

To gain experience with assays commonly used in therapy studies in preclinical models *in vitro*, two variants of the TNBC cell line MDA-MB468 were used: paclitaxel-sensitive, further referred to as PS and paclitaxel-refractory, further referred to as PR.

The sensitivity of PS and PR cells to paclitaxel was evaluated by three different assays: i) cell growth measured as cell confluence by the Incucyte S3, and cell viability scored by measurements for cellular metabolic activity: ii) MTS, reflecting NADH and NADPH and iii) CTG, reflecting quantity of ATP. Figure 11A shows changes in cell confluence over time in untreated controls and upon treatment with 4 nM of paclitaxel. Control PS and PR showed similar increase in cell confluence, and paclitaxel reduced the proliferation in both PS and PR. However, treated PR still showed higher cell confluence than the treated PS. To calculate the magnitude of treatment-induced growth inhibition, relative area under the curve (AUC) was calculated. The AUC values indicated that 4 nM of paclitaxel reduces the growth by 63% in PS cells and by 39% in PR (Figure 11B), validating that PR cells do show decreased sensitivity to paclitaxel. The MTS assay also shows that there are more viable cells in the treated PR samples, compared to the treated PS (Figure 11C). However, the viability decreases with increasing concentration of paclitaxel in both PS and PR. Similarly, the CTG assay also indicates reduced viability with increasing drug concentrations, where the treated PR were more viable than the treated PS (Figure 11D). In summary, it was validated by three different assays, that PR cells are less sensitive to paclitaxel, although they are not completely resistant.

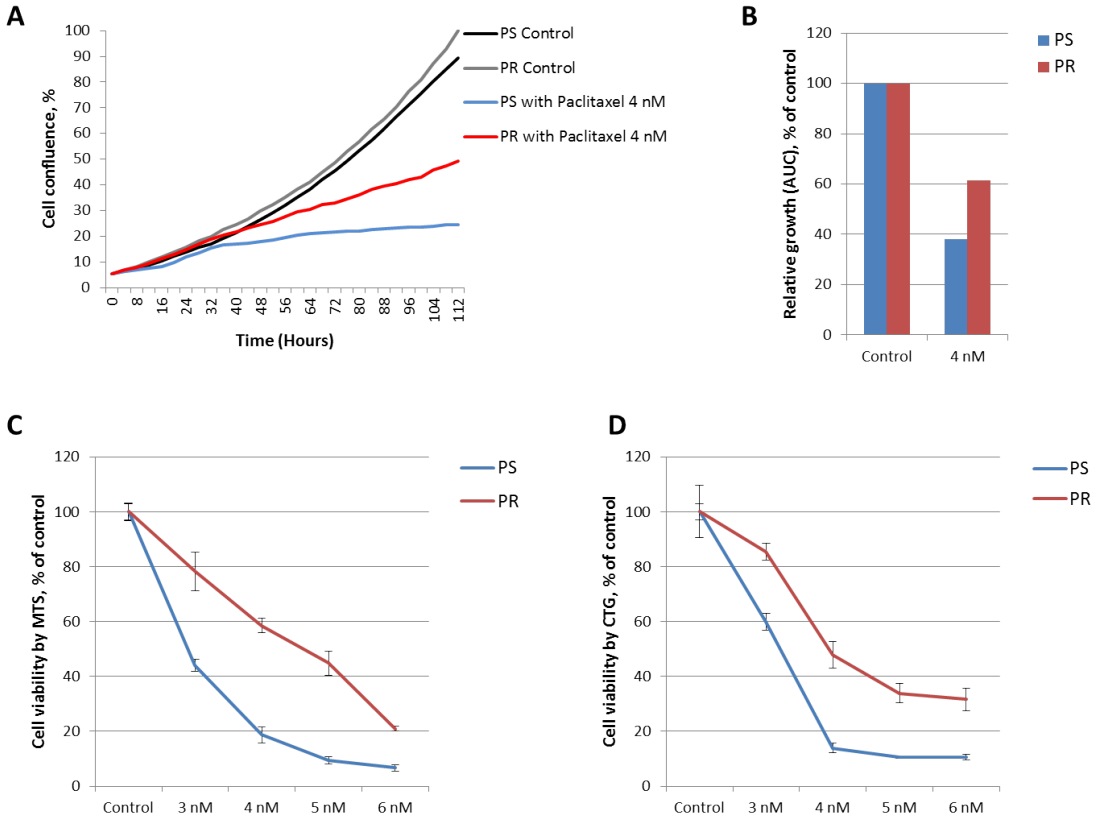

Figure 11: Effect of paclitaxel treatment in paclitaxel-sensitive (PS) and -refractory (PR) MDA-MB468 cells. **A:** Growth curves presented as cell confluence, measured by the Incucyte S3 and normalized to the confluence on day 0. The cells were exposed to paclitaxel for 4 days. **B:** Relative AUC calculated based on the growth curves from A, normalized to AUC-values in respective controls. **C:** and **D:** Cell viability was measured by the MTS and CTG assays on PS and PR cells treated with the indicated concentrations of paclitaxel for 4 days. Average ± StDv (n=6).

4.1.2 *Ex vivo* preclinical models

To gain experience with assays used for therapy studies in PDXCs, the tissue from paclitaxel-sensitive and -resistant sublines of MAS98.12 PDX was employed. MAS98.12 was the PDX model that was used when the PDXC method was developed in the group [74], and therefore it was the preferred model when learning the procedures. The tissue from both PDXs were dissociated to small fragments and further cultured in matrigel in 3D, as previously described. The fragments are further referred to as PDXCs. Both PDXCs were treated with 10 nM paclitaxel for 6 days (the controls were left untreated). Two methods were utilized to evaluate the treatment efficacy. First, it was attempted to measure the tissue growth by measuring fragment area by the Incucyte S3. Figure

12A and B shows the increase in fragment area with time, revealing a small effect of paclitaxel in the PDXC from the sensitive MAS98.12 (Figure 12A), but not from the resistant MAS98.12PR (Figure 12B). However, the growth rate was very low (1,2-1,6 fold increase), and there were big variations in the measured values, resulting in non-smooth growth curves that were difficult to interpret. This corresponds with previous observations in the group, where it was concluded that it was challenging to analyze MAS98.12-derived fragments by the Incucyte S3 [74].

Another tested method was based on live/dead staining followed by microscopic analysis of the cultures. As shown previously by the group [74], this method was well suited for the MAS98.12-derived PDXCs. Untreated and paclitaxel-treated PDXCs were stained with Calcein-AM and PI, allowing to visualize live and dead cells, respectively, by microscopy. As shown in Figure 12C, the untreated fragments were mostly live (green), even though there is a significant amount of dead (red) cells in the periphery of the fragments. Paclitaxel seemingly reduced the size of the live fragments, indicating the treatment influence. However, based on these images it was difficult to conclude whether the effect was bigger in PDXCs from MAS98.12, than MAS98.12PR. Since our aim was not to explore the treatment effect in MAS98.12-derived tissue, but rather to get familiar with the assays and procedures, no further quantification or repetition of the experiment was performed.

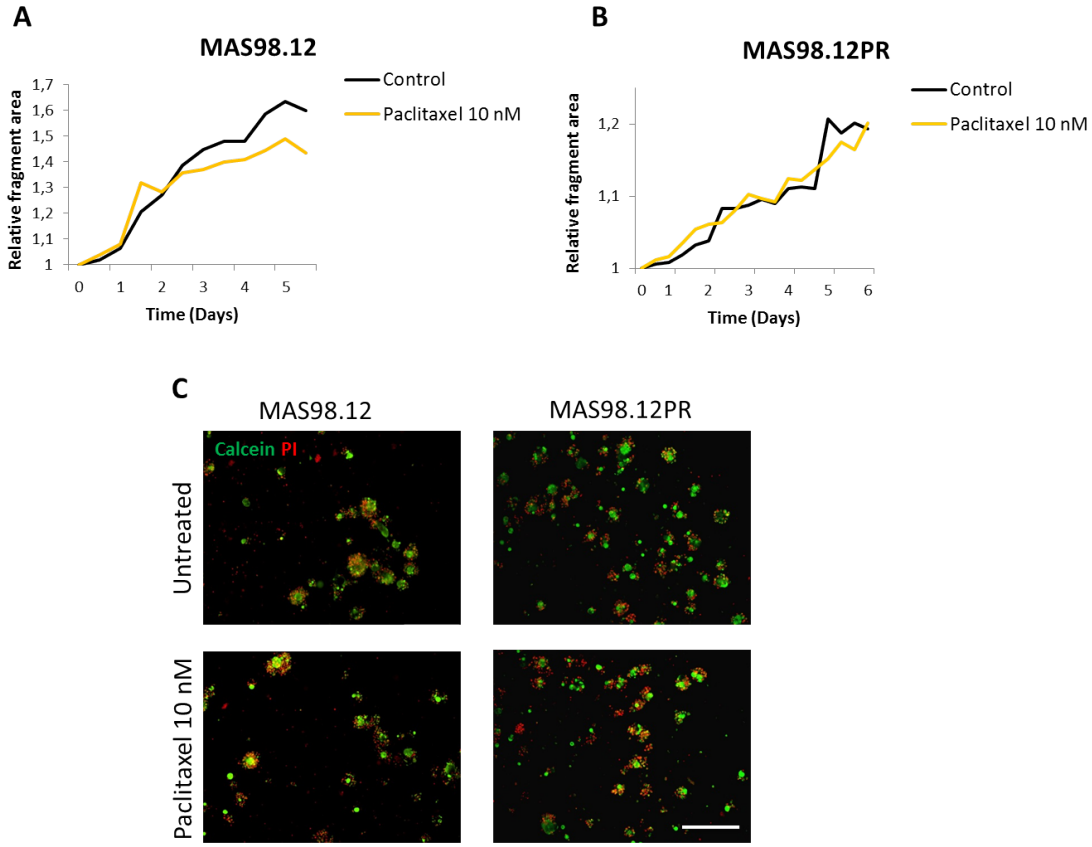

Figure 12: Untreated and paclitaxel-treated (10 nM for 5-6 days) PDXCs from MAS98.12 and MAS98.12PR were analyzed by: **A:** and **B:** measuring fragment size over time by the Incucyte S3, the values were normalized to the fragment area at day 0. **C:** Representative images of MAS98.12- and MAS98.12PR-derived PDXCs treated with paclitaxel for 5-6 days, followed by live/dead staining. Scale bar: 500 µm.

4.1.3 Immunostaining

Since the aim of this MSc project was to explore *ex vivo* drug sensitivity of the HBCx39 PDX-derived tissue, we performed initial characterization of these cultures via immunostaining. Another reason for such analysis was to get familiar with the immunostaining technique for later studies (see chapter 4.4). HBCx39 PDXCs were cultured for 10 days before they were fixed and immunostained for Epithelial Cell Adhesion Molecule (EpCAM) and Ki67. EpCAM is a transmembrane glycoprotein, which is expressed on most epithelial cells. Ki67 is a proliferation marker, allowing to get an idea about the proliferation levels of the fragments. As seen in Figure 13, we confirmed that the cultured fragments are positive for EpCAM, indicating that they consist of cells of epithelial origin, i.e. breast cancer cells. Only some areas within the

fragments were positive for Ki67, indicating their heterogenous composition where only a fraction of the cells were proliferating. The big blue stain outside of the fragments is an artifact of Hoechst, which was used to identify the nuclei.

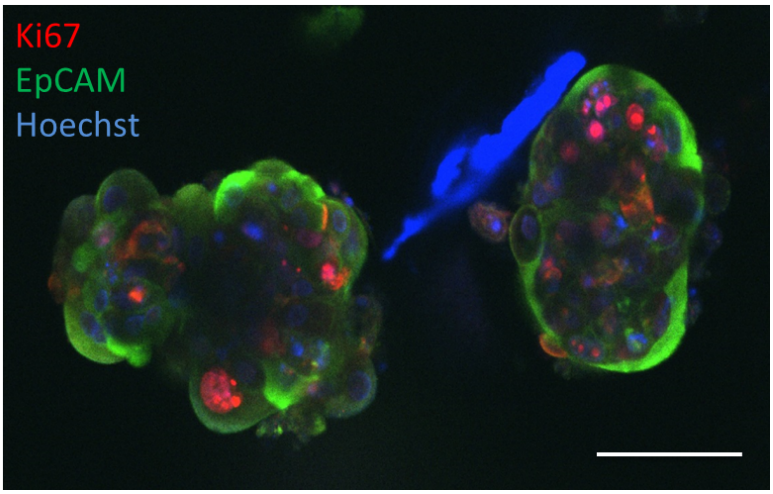

Figure 13: HBCx39-derived PDXCs immunostained for Ki67 (red), EpCAM (green) and nuclear staining (Hoechst in blue). Image representing the maximum intensity projection of all z-stacks, i.e. all captured z-stacks overlayed. Scale bar: 100 µm.

4.2 Analysis of HBCx39 PDX-tissue sensitivity to anti-cancer drugs *ex vivo*

To evaluate the sensitivity of anti-cancer drugs *ex vivo*, the HBCx39 PDX-tissue was used. This PDX was chosen because of its suitability to several read-out methods. Three methods were used in the evaluation: monitoring of fragment-area by the Incucyte S3, cell viability assay (CTG) and live/dead staining followed by microscopic analysis.

For the ADCs, Enhertu and Trodelvy, the dose response on PDXCs had not been evaluated before in the group. To decide which doses were the most effective, several doses were tested on HBCx39-derived PDXCs. To evaluate the dose response to Enhertu *ex vivo* in the tissue from HBCx39 PDX, we established the PDXCs and treated them with 10 nM, 100 nM and 1000 nM of Enhertu for 9 days. The effect was evaluated by measuring fragment area by Incucyte S3 and by live/dead staining. As shown in Figure 14A, the response was dose-dependent, as the relative fragment area decreases with increased concentration of Enhertu. Enhertu at 10 nM hardly had any effect, while the

effect of 1000 nM was the most obvious. After 9 days of Enhertu-exposure, the PDXCs were stained with Calcein-AM and PI, to visualize the live and dead cells, respectively (Figure 14B). It is observed both a decrease in the size of live (green) fragments and an increase in the dead (red) cells in the periphery of the fragments, upon increased concentration of Enhertu. Also here, the effect was the most obvious in the 1000 nM Enhertu-treated PDXCs.

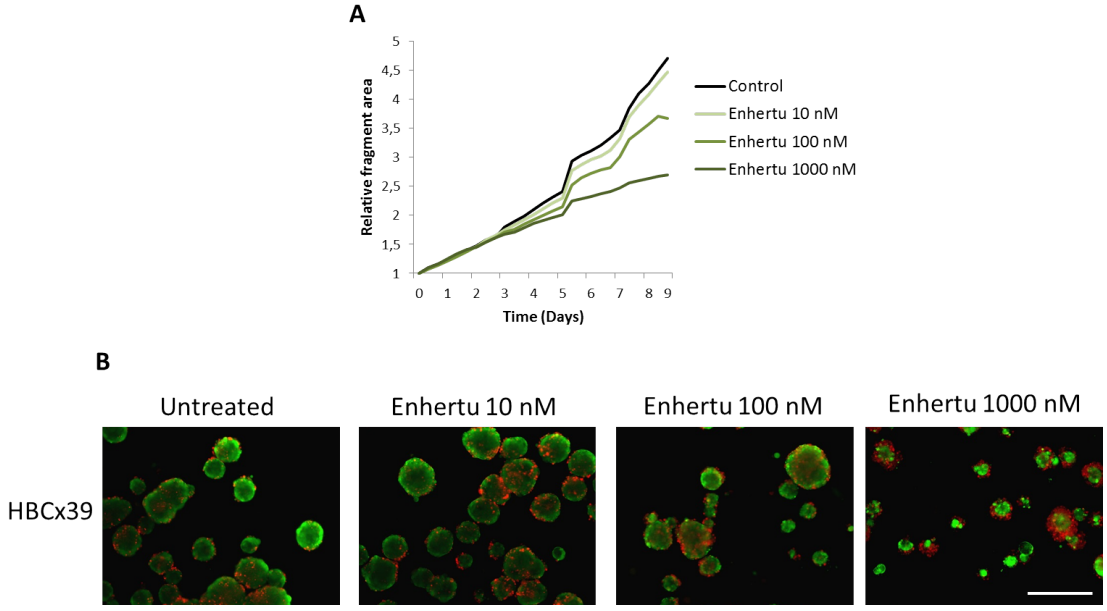

Figure 14: **A:** HBCx39-derived PDXCs treated with Enhertu 10 nM, 100 nM and 1000 nM for 9 days. Fragment area measured by the Incucyte S3, and normalized to the fragment area at day 0. **B:** Representative images of HBCx39-derived PDXCs treated with Enhertu 10 nM, 100 nM and 1000 nM for 9 days, followed by live/dead staining. Scale bar: 500 µm.

Similarly, we also assessed the dose response to Trodelvy. PDXCs from HBCx39 were treated with 1 nM, 10 nM and 100 nM of Trodelvy and the effect was measured as described above. It is observed a dose-dependent response to Trodelvy, with the fragment area decreasing with increased concentration of Trodelvy (Figure 15A). Trodelvy at 100 nM induced the most notable effect. The same trend is seen in the live/dead images, where the PDXCs treated with 100 nM of Trodelvy have the lowest proportion of live (green) area and the highest proportion of dead (red) cells (Figure 15B).

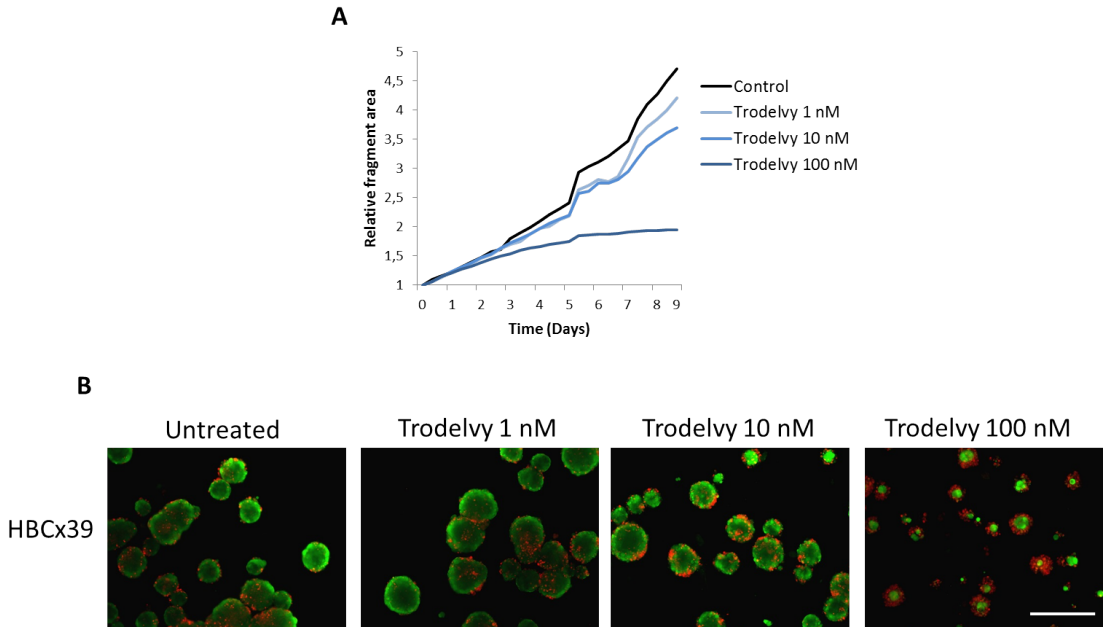

Figure 15: **A:** HBCx39-derived PDXCs treated with Trodelvy 1 nM, 10 nM and 100 nM for 9 days. Fragment area measured by the Incucyte S3, and normalized to the fragment area at day 0. **B:** Representative images of HBCx39-derived PDXCs treated Trodelvy 1 nM, 10 nM and 100 nM for 9 days, followed by live/dead staining. Scale bar: 500 µm.

To assess the HBCx39 tissue response to different anti-cancer treatments *ex vivo*, a drug sensitivity assessment screen consisting of 4 drugs was set up. The PDXCs were exposed to Enhertu, Trodelvy, paclitaxel and everolimus for 8-9 days. We used 1000 nM Enhertu and 100 nM Trodelvy based on the dose response data (Figure 14 and 15), while 10 nM paclitaxel and 20 nM everolimus were chosen from previous experience with MAS98.12 PDXCs [74]. Furthermore, paclitaxel and everolimus were effectively suppressing the growth *in vivo* in the HBCx39 PDX [74]. Figure 16A shows two representative experiments, where the same drug sensitivity assessment screen was performed in PDXCs generated from different individual tumors at different days. There is observed a clear variance between the two experiments, with respect to the growth of the untreated fragments. In experiment 1, we observed a 4,7-fold increase in fragment area, while only a 1,7-fold increase was observed in experiment 2, indicating a slower growth in the latter. Despite this difference, we observed a clear treatment-induced reduction of fragment growth in both experiments.

To merge the Incucyte-data from all performed experiments, we calculated AUC for each treatment and controls in each experiment. AUC-values from the treated samples

were normalized to the AUC-values in the untreated controls (set to 100%), revealing the magnitude of the treatment-induced growth inhibition. Figure 16B presents the average of the AUC values from 2-5 experiments (n is different for each drug). The strongest observed response was to 20 nM everolimus and 10 nM paclitaxel, which reduced the fragment growth to 21% and 35% respectively, compared to the untreated controls. Both 1000 nM Enhertu and 100 nM Trodevy reduced the growth to approximately 65% compared to the controls (Figure 16B).

To visualize the treatment-induced effect, live/dead staining was performed, as presented in Figure 16C. PDXCs treated with everolimus show a significant decrease in the size of live (green) fragments without appearance of dead (red) cells. Everolimus is a cytostatic drug, which means that it impairs growth of cancer cells instead of inducing cell death. On the contrary, paclitaxel is a cytotoxic drug, inducing cell death in cancer cells. Thus, upon paclitaxel-treatment, PDXCs respond with an accumulation of dead (red) cells in the periphery of the fragments, and the area of the live (green) fragments was also reduced (Figure 16C). For Trodelvy and Enhertu, it is observed both a decrease in the size of live (green) fragments and an increase in dead (red) cells, which indicates both cytostatic and cytotoxic influence of these drugs (Figure 16C).

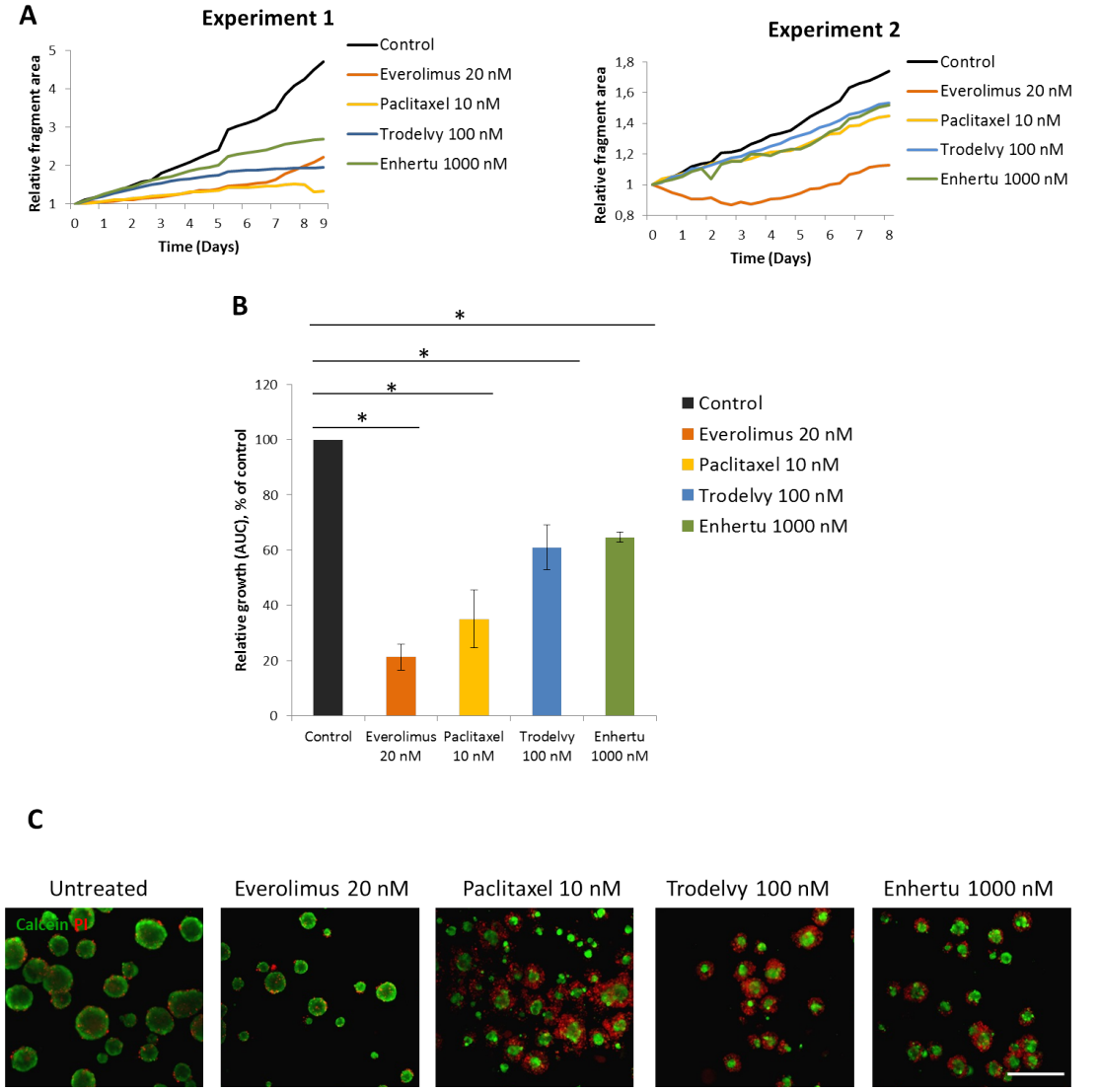

Figure 16: **A:** Two independent experiments performed on HBCx39-derived PDXCs treated with 20 nM everolimus, 10 nM paclitaxel, 100 nM Trodelvy and 1000 nM Enhertu. The PDXCs were incubated with the drugs for 8-9 days. Fragment area was measured by the Incucyte S3, and normalized to the fragment area measured on day 0. **B:** AUC calculated from data measured by the Incucyte S3, normalized to the untreated control. The figure represents the average of the AUC values calculated from 2-5 experiments. Average ± SEM (n≥3). *, $p < 0.05$ by unpaired t-test. **C:** Representative images of HBCx39-derived PDXCs from experiment 1 treated with drugs for 9 days, followed by live/dead staining. Scale bar: 500 µm.

To verify the results from the Incucyte S3, CTG was performed after treatment for 9 days (Figure 17). For everolimus and paclitaxel, the results are quite similar to those seen in Figure 16B, i.e. the viability is reduced to 20-35%. Trodelvy and Enhertu reduced the viability to approximately 40%, which indicates a stronger effect than measured by

the Incucyte S3/AUC values in Figure 16, although a large SEM should be noted. This might be due to methodological reasons (discussed in chapter 5.3.2). Thus, generally, the Incucyte S3 and the CTG assays provide comparable information about HBCx39-tissue sensitivity.

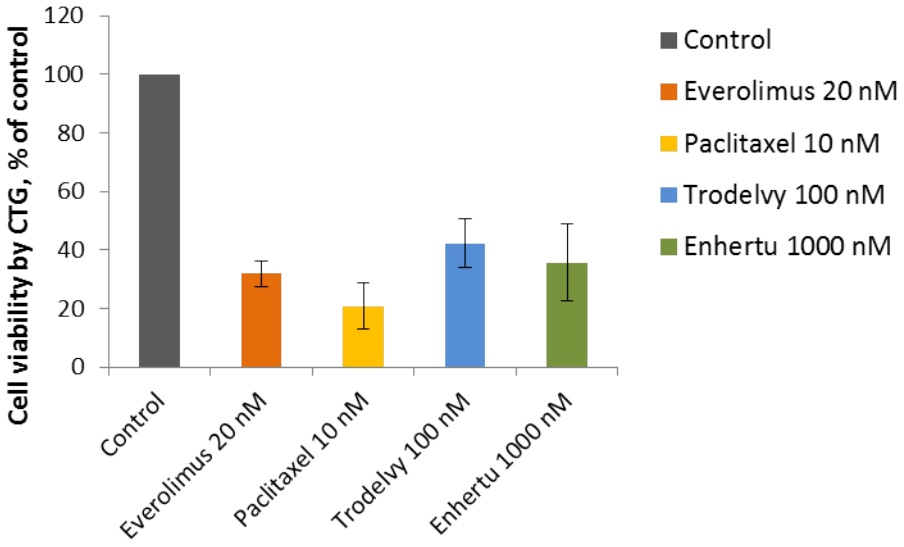

Figure 17: HBCx39-derived PDXCs response to everolimus 20 nM, paclitaxel 10 nM, Trodelvy 100 nM and Enhertu 1000 nM scored by measuring metabolic activity. The PDXCs were treated with the indicated drugs for 9 days before treatment effect was measured by the CTG assay. The values in the treated cultures are presented as percentage of the untreated control. Average ± SEM (n=3).

To assess how the tumor-tissue from the Enhertu-resistant PDX, HBCx39ER, responds to anti-cancer drugs, we established the respective PDXCs that were treated with the same drug sensitivity assessment screen as HBCx39 PDXCs for 9-10 days. Figure 18A shows the results from two representative experiments, where the PDXCs were established from different tumors on different days. The growth of the untreated fragments was quite similar in both experiments, resulting in a 2,1-2,2-fold increase in fragment area. 1000 nM Enhertu and 100 nM Trodelvy did not induce any effect in experiment 1, while in experiment 2 we observed a small effect for the Enhertu-treated PDXCs, and a slightly bigger effect for the Trodelvy-treated. The effect of paclitaxel was also quite low in experiment 1, and slightly bigger in experiment 2. Only everolimus induced a clear growth inhibition in both experiments. We merged the results from 2-5 experiments by calculating relative AUC values, as described above. As shown in Figure 18B, Enhertu-treated fragments have a relative growth of 96% and Trodelvy-treated

fragments have a relative growth of 83% as compared to the untreated controls, but this reduction was not statistically significant. Paclitaxel reduced the growth to 66%, but also this effect was not statistically significant due to relatively high SEM. The same applies to everolimus.

In addition, live/dead staining was performed on PDXCs from experiment 2 to visualize the treatment effect. The drug responses measured by the Incucyte S3 was validated by the live/dead staining, as shown in Figure 18C. The Enhertu-treated fragments are quite similar to the controls regarding the size of the live (green) area, but they contain some dead (red) cells in the periphery. The live (green) area of the fragments treated with the other drugs were reduced, especially in the case of everolimus.

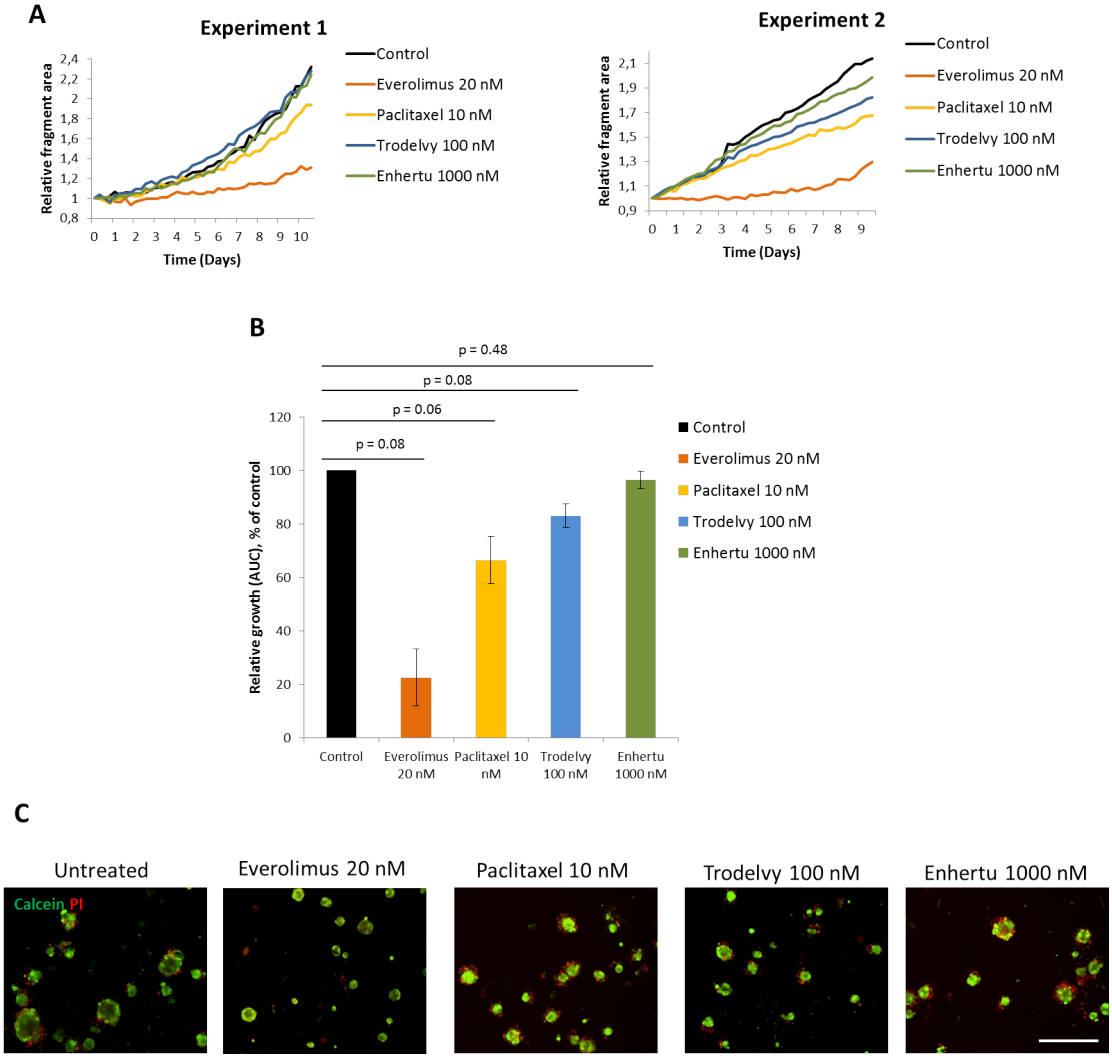

Figure 18: **A:** Two independent experiments performed on HBCx39ER-derived PDXCs treated with 20 nM everolimus, 10 nM paclitaxel, 100 nM Trodelvy and 1000 nM Enhertu. The PDXCs were incubated with the drugs for 9-10 days. Normalized to fragment area at day 0. **B:** AUC calculated from data measured by the Incucyte S3, normalized to untreated control. The figure represents the average of the AUC values calculated from several experiments. Average ± SEM (n≥3 for paclitaxel, Trodelvy and Enhertu) and ± StDv (n=2 for everolimus). P-values calculated by unpaired t-test, comparing each drug with the untreated control. **C:** Representative images of HBCx39ER-derived PDXCs from experiment 2 treated with drugs for 9 days, followed by live/dead staining. Scale bar: 500 µm.

4.3 Comparing drug-sensitive and drug-resistant PDXC models

For easier comparison between the treatment-induced effects in tissue from HBCx39 and HBCx39ER, we generated Figure 19 (with data from Figure 16B and 18B). The figure illustrates the difference in the PDXCs sensitivity, revealing that the tissue from the Enhertu-resistant tumor was less/not responsive to paclitaxel, Trodelvy and Enhertu. Unfortunately, only in the case of Enhertu, the difference was statistically significant, where the drug decreased the growth by 35% and 4% in HBCx39- and HBCx39ER-PDXCs, respectively. In the case of 100 nM Trodelvy, the difference was obvious (reduction by 39% versus 17%) but it did not result in statistical significance (p=0,08), although the same tendency was observed also at the 10 nM concentration (reduction by 18% versus 8%). Also sensitivity to paclitaxel was clearly different (reduction by 65% versus 34%), but it did not result in statistical significance based on the experiments in this project. In summary, this data indicates that the tissue from the Enhertu-resistant tumors is insensitive to Enhertu and less sensitive to Trodelvy and paclitaxel.

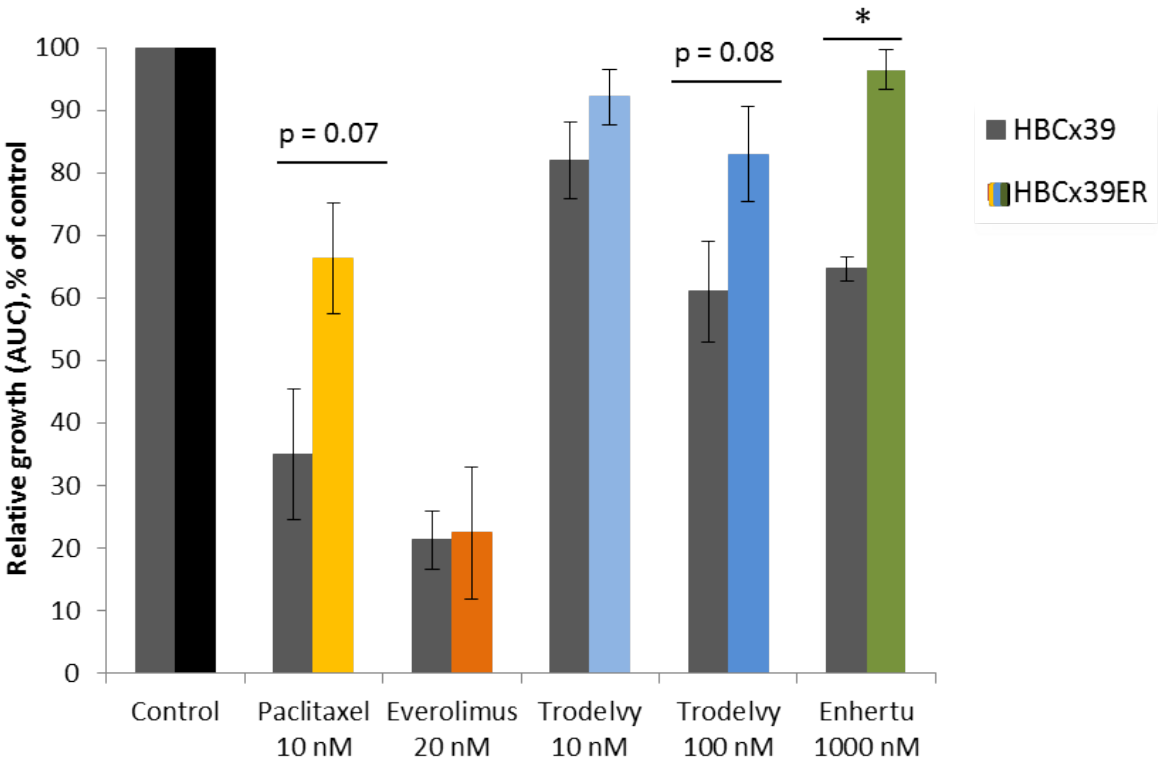

Figure 19: AUC calculated from data measured by the Incucyte S3, normalized to the respective untreated controls. The values presented in the figure are the average of 2-5 experiments, and reflects the overall growth of the organoids. The parental model of the HBCx39-derived PDXCs is shown in grey, while the Enhertu-resistant subline is shown in colors corresponding to the different drugs. Average ± SEM (n≥3 for paclitaxel, Trodelvy, Enhertu and everolimus on HBCx39) and ± StDv (n=2 for everolimus on HBCx39ER). *, $p < 0{,}05$ by unpaired t-test. Remaining p-values were calculated by unpaired t-test, comparing the drug response of HBCx39- and HBCx39ER-PDXCs.

4.4 Exploration of possible resistance mechanisms

To assess possible mechanisms of resistance, we considered several possibilities: i) impaired sensitivity to inhibition of topoisomerase I (the action of the payloads in Enhertu and Trodelvy), ii) reduced level of the ADC-binding receptors, i.e. HER2 and Trop-2, and iii) altered levels of the molecules involved in the ADC internalization, the endocytic pathway, e.g. RAB5.

To investigate whether the resistance observed in HBCx39ER could be associated with the impaired response to topoisomerase I inhibition, we used another topoisomerase

I inhibitor, irinotecan. Irinotecan is not an ADC and its active metabolite is identical with the payload of Trodelvy (SN-38) [83]. Thus, we established PDXCs from HBCx39 and HBCx39ER, treated them with different concentrations of irinotecan and compared the tumor sensitivity. As shown in Figure 20A and B, there is not observed a notable difference in the sensitivity between HBCx39- and HBCx39ER-PDXCs. Both tissues respond quite weakly. 2 µM of irinotecan induced a 18% and 26% decrease in growth in HBCx39- and HBCx39ER-PDXCs, respectively. Upon treatment with 5 µM of irinotecan, both HBCx39 and HBCx39ER have approximately a 24% decrease in growth. No obvious difference was seen from the live/dead images either (Figure 20C).

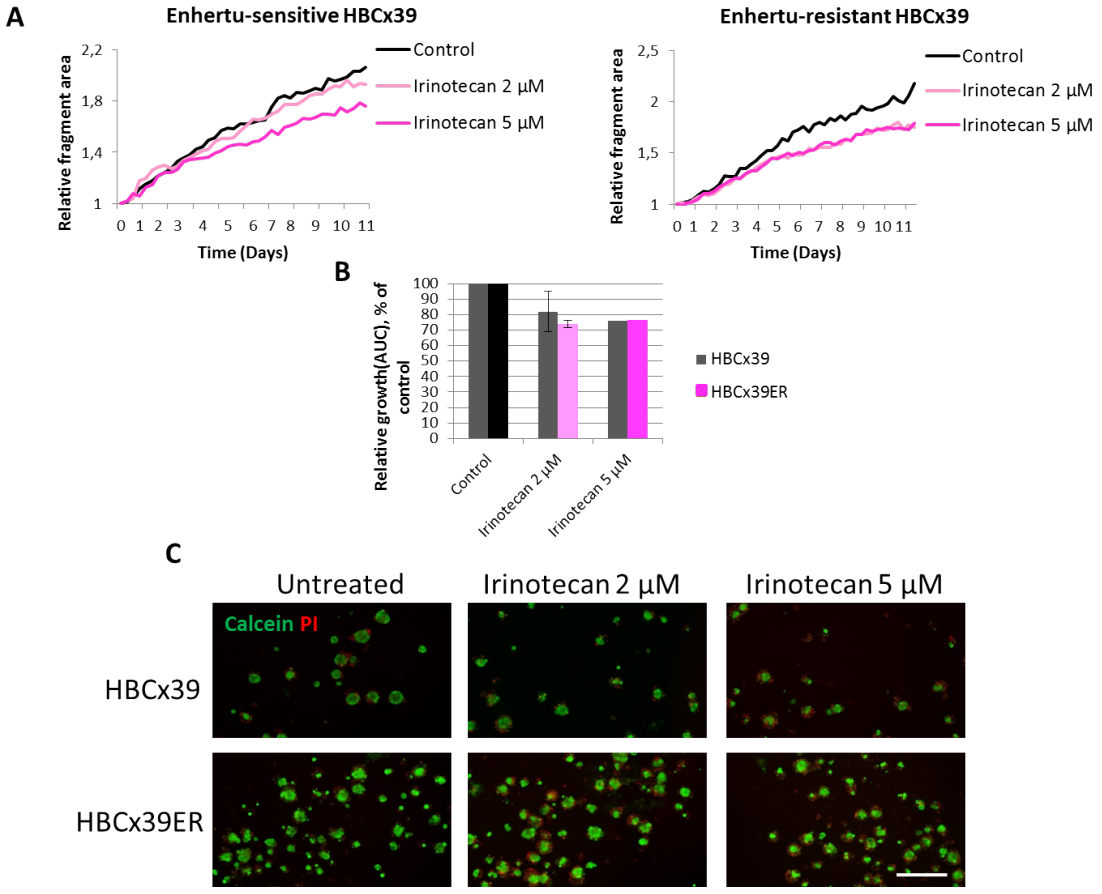

Figure 20: **A:** HBCx39- and HBCx39ER-derived PDXCs treated with irinotecan 2 µM and 5 µM for 11 days. Normalized to the fragment area measured on day 0. **B:** AUC calculated from data measured by the Incucyte S3, normalized to the untreated control. Average ± StDv (n=2, n=1 for irinotecan 5 µM). **C:** Representative images of HBCx39- and HBCx39ER-derived PDXCs treated with irinotecan 2 µM and 5 µM for 11 days, followed by live/dead staining. Scale bar: 500 µm.

To explore whether the resistance might be associated with alterations in HER2 and Trop-2 levels, we employed immunofluorescence. PDXCs from the Enhertu-sensitive and resistant HBCx39 were immunostained for HER2 and Trop-2 in order to asses if HER2 and Trop-2 are differently expressed in the two tissues. We hypothesized that there could be less expression of HER2/Trop-2 in HBCx39ER, as a decrease in receptor-expression has been linked to ADC-resistance [21]. Comparing the HER2-staining in HBCx39 and HBCx39ER in Figure 21, there is not observed a difference in expression. Furthermore, all fragments and all cells within the fragment showed similar expression indicating relatively uniform levels among and within the fragments. Similarly, no difference of expression of Trop-2 between HBCx39 and HBCx39ER was observed (Figure 22). In addition, the PDXCs were stained with panCK, a marker of epithelial cells [84], to be sure that the analyzed fragments represents breast cancer tissue. As seen in Figure 21 and 22, both HBCx39 and HBCx39ER uniformly express panCK throughout the fragments, indicating that the fragments are indeed composed of tumor cells of epithelial origin. The lack of staining in the core of the fragments in Figure 22 is most likely due to methodological considerations (discussed in chapter 5.3.3).

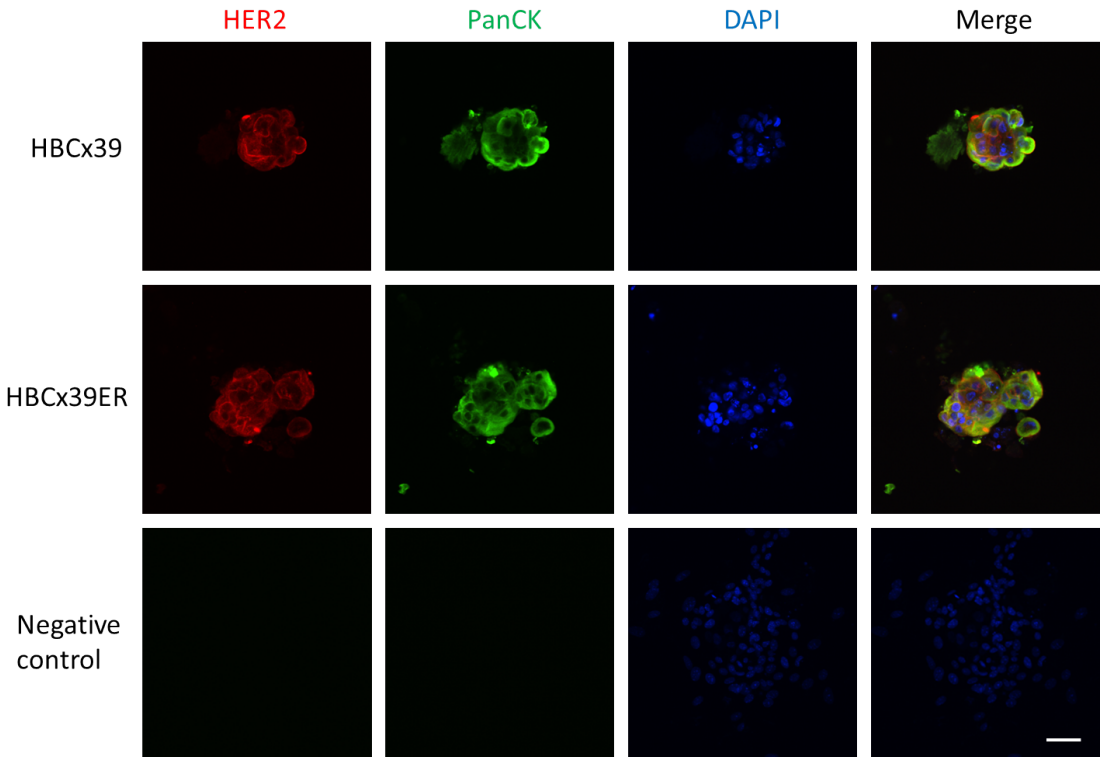

Figure 21: HBCx39- and HBCx39ER-derived PDXCs immunostained for HER2 (red), PanCK (green) and nuclear staining (DAPI in blue). Scale bar: 50 µm.

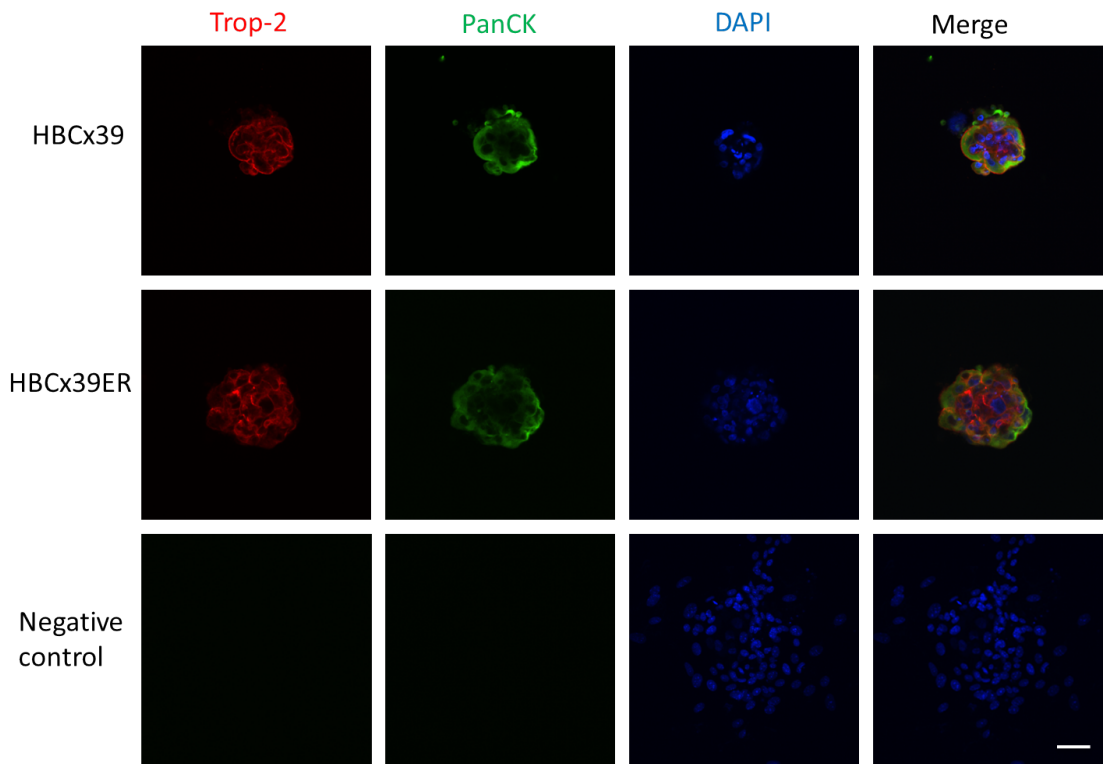

Figure 22: HBCx39- and HBCx39ER-derived PDXCs immunostained for Trop-2 (red), PanCK (green) and nuclear staining (DAPI in blue). Scale bar: 50 µm.

To evaluate the level of HER2 and Trop-2 in the treated tissue, the PDXCs were exposed to 1000 nM Enhertu and 100 nM Trodelvy for 10 days before they were fixed and immunostained for HER2, Trop-2 and PanCK. As seen in Figure 23 and 24, both HER2 and Trop-2 is uniformly expressed throughout the fragments of the treated PDXCs. As discussed in chapter 5.3.3, the expression levels might seem higher in the smaller fragments, but this is most likely due to methodological reasons.

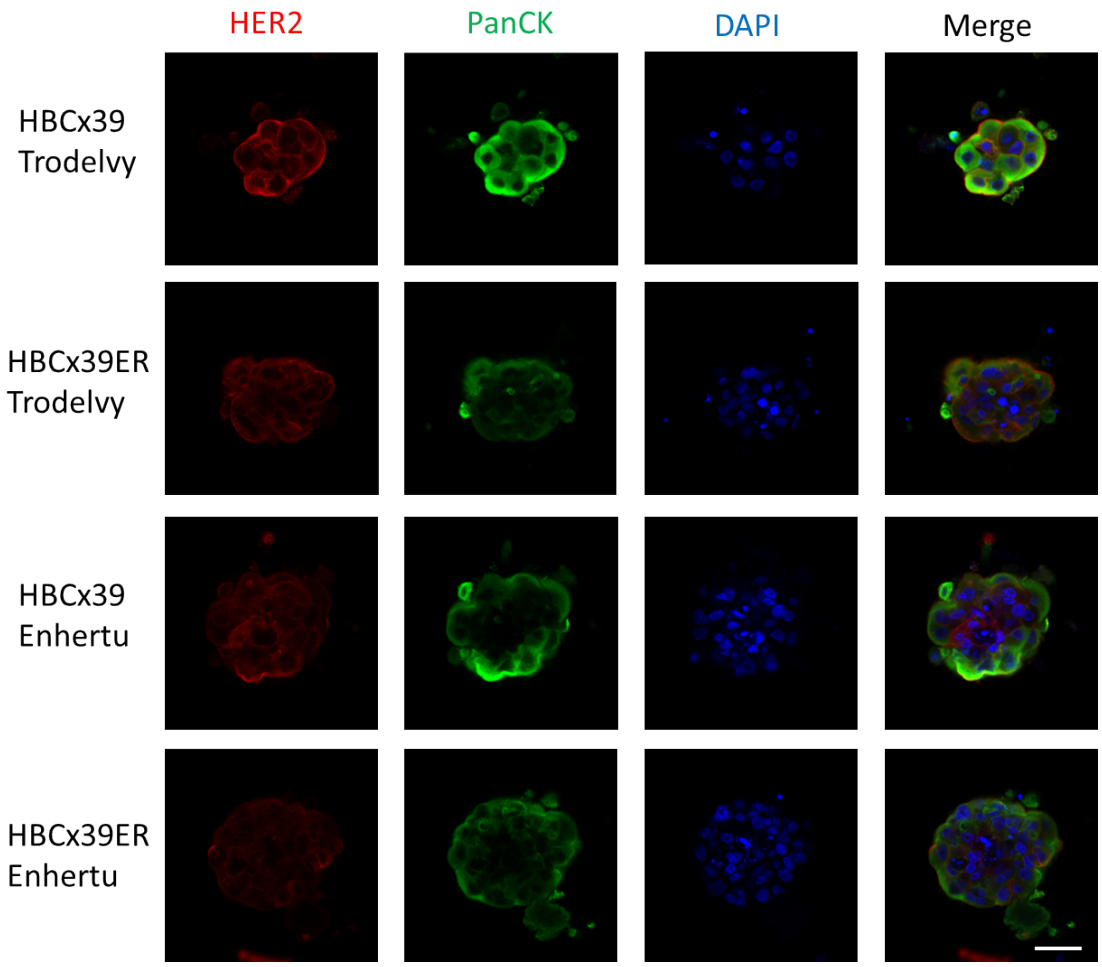

Figure 23: HBCx39- and HBCx39ER-derived PDXCs treated with Trodelvy 100 nM and Enhertu 1000 nM for 10 days. Immunostained for HER2 (red), PanCK (green) and nuclear staining (DAPI in blue). Scalebar: 50 µm.

To evaluate whether the Enhertu-resistance could be associated with RAB5-levels, we planed to stain both the HBCx39- and HBCx39ER PDXCs for RAB5. To assess whether we could detect the signal that resembles the expected RAB5-staining, we first employed HBCx39-derived PDXCs. HBCx39 is highly sensitive to Enhertu, and this sensitivity might be associated with RAB5-expression, as reported in [52]. As RAB5 is an early endosome marker, it is expected to be detected as small dots in the IF images. As shown in Figure 25, we observed weak, red dotted staining inside the fragments (indicated by white arrows), specifically in the area around the nuclei, which might be an indication of RAB5. However, we also observed some dotted staining in the periphery of the fragments (indicated by blue arrows), as well as outside of the fragments. Also, a notable amount of unspecific staining was observed in the core of the fragment, but this

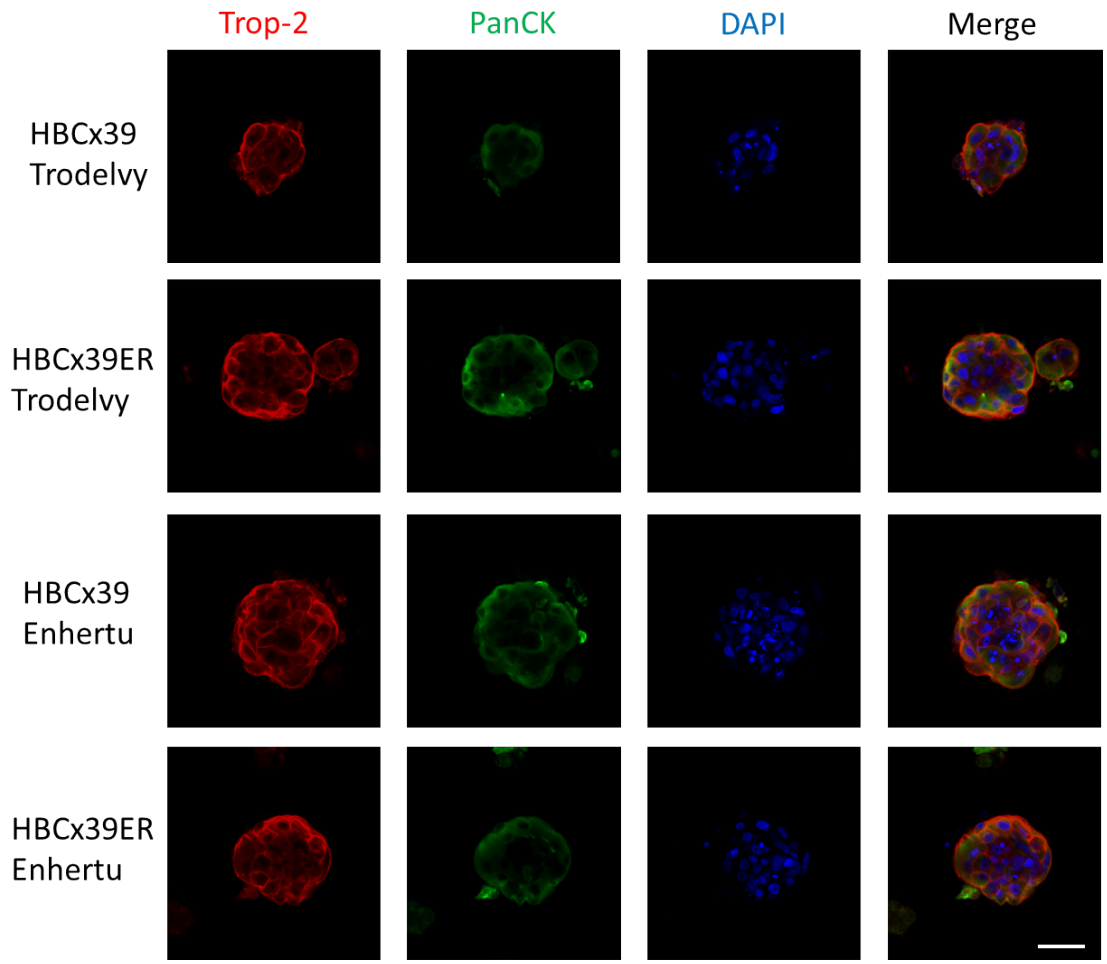

Figure 24: HBCx39- and HBCx39ER-derived PDXCs treated with Trodelvy 100 nM and Enhertu 1000 nM for 10 days. Immunostained for Trop-2 (red), PanCK (green) and nuclear staining (DAPI in blue). Scalebar: 50 µm.

is most likely due to methodological reasons. Although it was a promising pattern, we concluded that the experiment required further optimization and costaining with known markers of early endosomes (e.g. EEA1). Unfortunately, due to time limitations, no further optimization nor staining of the HBCx39ER-derived PDXCs were performed.

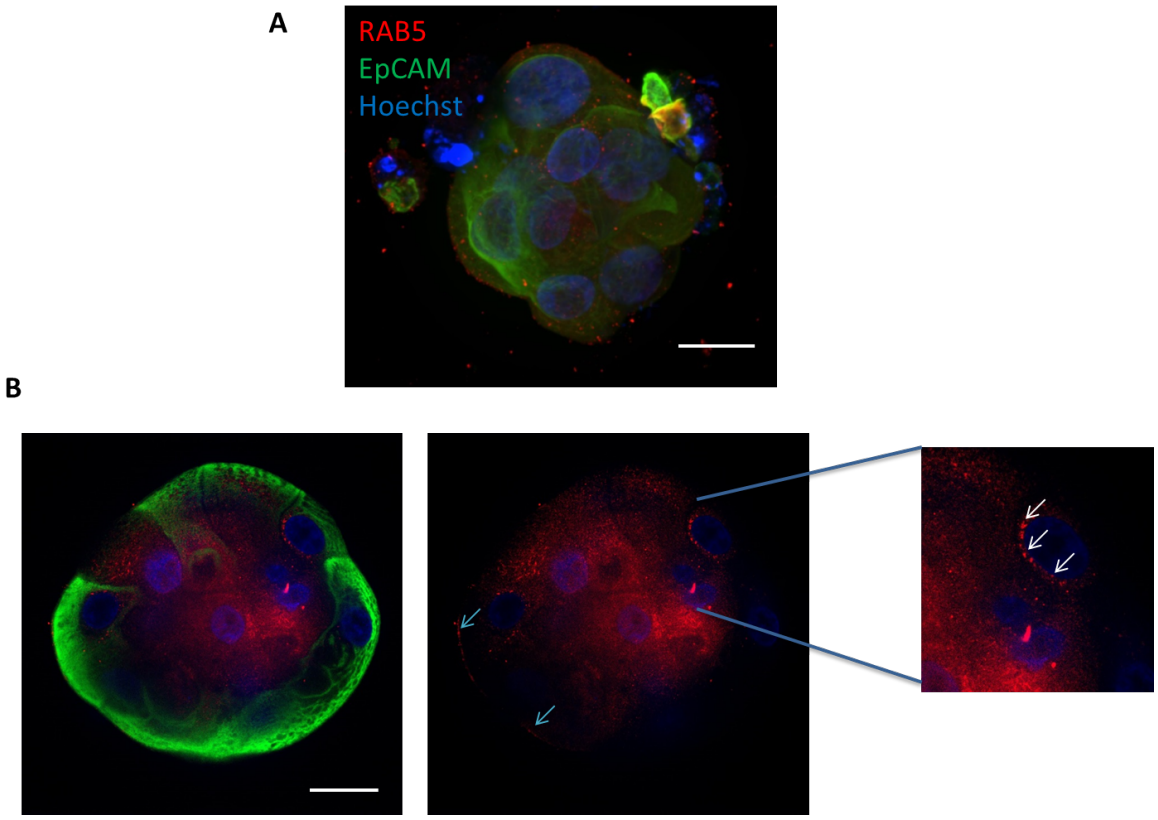

Figure 25: HBCx39-derived PDXC immunostained for RAB5 (red), EpCAM (green) and nuclear staining (Hoechst in blue). **A:** Image representing the maximum intensity projection of all z-stacks, i.e. all captured z-stacks overlayed. **B:** Images representing one z-stack in the middle of the fragment. The left image shows all colors merged, and the middle image shows RAB5 (red) and nuclear staining (Hoechst in blue) merged. The right image is zoomed in on the specific cell where the dotted staining is observed. Scale bar: 25 µm.

Discussion

Patients with TNBC have a high likelihood of recurrence after initial treatment [85]. Novel drugs, like ADCs, show great promise in the effective treatment of BC patients who have already been exposed to other forms of treatment [86]. TNBCs are especially challenging to treat, because of the lack of druggable targets on the cancer cells. Recently, two ADCs have been approved for the treatment of TNBC [87].

In this project, these ADCs, Enhertu and Trodelvy, in addition to other anti-cancer drugs, have been tested *ex vivo* on cultured tumor tissue from PDXs with distinct sensitivity to Enhertu. Several methods were used to evaluate both drug responses and possible mechanisms of drug resistance by using PDXCs as a model.

5.1 The potential of PDXC to predict tissue sensitivity to treatment

In recent years, patient-derived tumor explants or organoids have emerged as attractive tools for evaluating tumor-tissue sensitivity to drugs *ex vivo* [88]. An important requirement for such an approach to be useful for functional precision diagnostics, is that the tissue sensitivity detected *ex vivo* should match the sensitivity of the tumors themselves. Such comparison between the tumor tissue drug sensitivity *in vivo* and *ex vivo* has been performed using the PDX-PDXC platform developed previously in our group [74]. It has been shown that drug sensitivity or resistance detected in PDXCs generally recapitulates the sensitivity/resistance seen *in vivo* [74], suggesting that the *ex vivo* platform can provide predictive information. This thesis further strengthens the potential of PDXCs to predict how the respective PDXs will respond to treatment. We have demonstrated that the tissue from Enhertu-resistant tumors, when cultured *ex vivo* as PDXCs, also do not respond to Enhertu. Furthermore, we demonstrated that PDXCs from the Enhertu-resistant tumors show lower sensitivity also to Trodelvy and

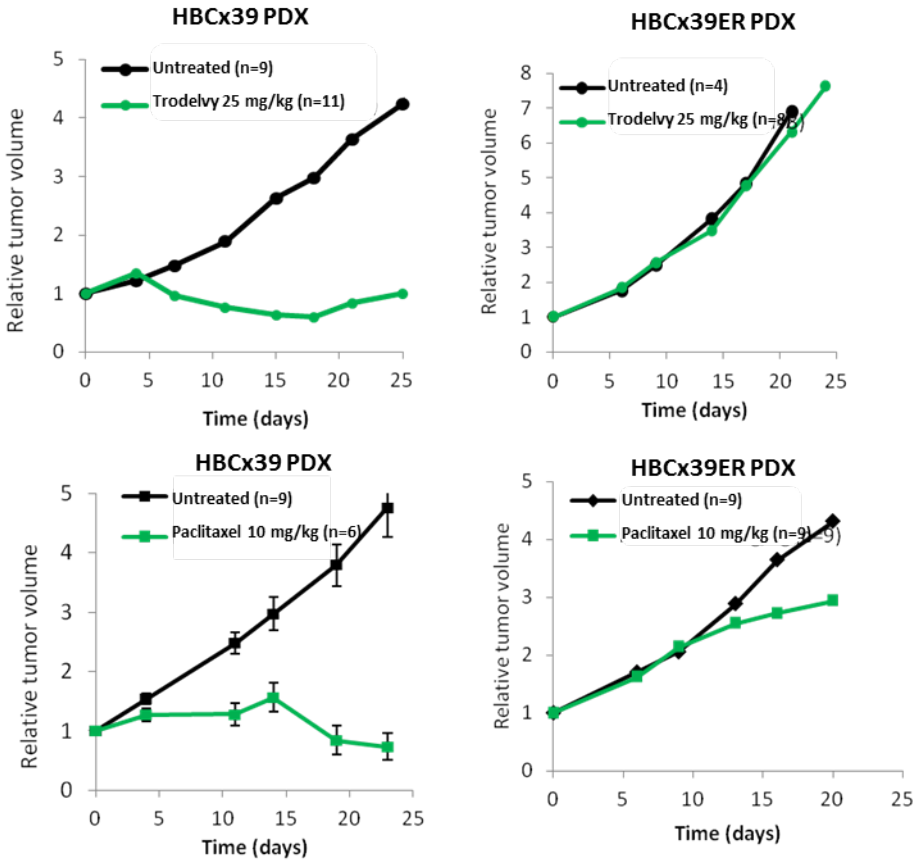

Figure 26: *In vivo* experiments performed after observing the response to Trodelvy and paclitaxel *ex vivo*. *In vivo* experiments performed by: Geir Frode Øy. Figure provided by: Lina Prasmickaite.

paclitaxel compared to PDXCs from Enhertu-sensitive tumors (Figures 16 and 18). This allowed us to predict that the HBCx39ER PDX should be less responsive to Trodelvy and paclitaxel when treated *in vivo*. This prediction was later validated by *in vivo* experiments performed by other members of the group (as shown in Figure 26). Based on the *in vivo* and *ex vivo* responses being comparable, we suggest that PDXCs can be used to substitute *in vivo* studies, at least in some cases. For example, therapy studies in PDXCs might help in choosing promising drugs for further investigation *in vivo*.

5.2 Evaluation of possible drug resistance mechanisms

The observation that PDXCs recapitulate the Enhertu-resistance seen *in vivo*, indicates that the resistance mechanisms are preserved and functional when the tissue is cultured *ex vivo*. Similarly, it has been demonstrated previously, that the multidrug

transporter (encoded by the *MDR1* gene), which was responsible for paclitaxel resistance in MAS98.12PR PDX, remained functional in the respective PDXCs [74]. Based on these observations, we anticipated that we could use PDXCs to explore possible mechanisms of resistance to the ADCs.

Since the first step in ADC internalization is binding to the targeted receptors on the cell surface, we started by investigating whether these receptors are present in the resistant PDXCs. We chose to use the IF method, since this allows for detection of expression level of the proteins, in addition to making it possible to visualize the localization of the proteins in the fragments. Additionally, IF allows for comparison of expression between fragments. Thus, both HBCx39- and HBCx39ER-derived PDXCs were analyzed by IF to detect HER2 and Trop-2 expression. We detected uniform and comparable levels of HER2 and Trop-2 in the PDXCs from sensitive and resistant tumors. This indicates that the resistance of HBCx39ER to Enhertu and Trodelvy is not related to loss of expression of these receptors. However, as reported in [62], truncated forms of HER2 has been associated with resistance to trastuzumab. This resistance mechanism could not be addressed by using the commercially available antibody as used in this IF experiment. A specific antibody that recognizes a truncated form of HER2 would be required for such detection. Such antibody has recently been developed, as reported in [89].

The fact that the Enhertu-resistant tissue was also less responsive to Trodelvy, both *ex vivo* and *in vivo*, suggests that HBCx39ER has developed a resistance mechanism that is common for both ADCs. One possibility is that the resistance mechanism involves the endocytic pathway, which is utilized by both Enhertu and Trodelvy to deliver their payload into the cell. To investigate the involvement of the endocytic pathway members, we stained HBCx39-derived PDXCs for RAB5. RAB5A is a protein that is involved in the delivery of cargo from the plasma membrane to early endosomes, as well as being involved in endosome fusion [52]. RAB5A expression has been found to have a strong correlation with sensitivity to the HER2-targeting ADC, Kadcyla, and can be used as a predictive biomarker for Kadcyla response [52]. On this basis, we considered the possibility that the resistant tissue might have low levels of RAB5. Unfortunately, this was not addressed in this project due to time limitations. However, we did analyze PDXCs from HBCx39 that have shown high sensitivity to Enhertu, suggesting that they should express RAB5. As shown in Figure 25, there is observed some dotted staining in the

area surrounding the nuclei, which might indicate RAB5 staining. Further experiments should be performed.

Another possible mechanism of resistance is the target of the payload. For both Enhertu and Trodelvy, the payloads inhibit topoisomerase I, so we hypothesized that insensitivity to topoisomerase I inhibition might be the reason for the ADC-resistance. Resistance to toposiomerase I inhibitors has been previously reported [90]. In order to test this hypothesis, we compared the sensitivity of PDXCs from HBCx39 and HBCx39ER to the topoisomerase I inhibitor, irinotecan. Irinotecan was chosen because it is not an ADC and therefore its activity should not depend on the upstream steps that are unique for ADCs. Thereby, we could compare whether the Enhertu-sensitive and -resistant tissues respond differently to toposiomerase I inhibition. There was not observed a notable difference in responsiveness to irinotecan between the two PDXCs (Figure 20). This indicates that this probably is not the resistance mechanism utilized by HBCx39ER. However, it should be noted that both PDXCs responded quite weakly to the treatment, which makes it difficult to observe the difference in responsiveness. Further drug sensitivity experiments with irinotecan, or some other topoisomerase I inhibitor, should be performed.

In conclusion, the studies of this project have not identified the biological mechanism that causes the resistance in the HBCx39ER tissue. But as described above, the possible involvement of the endocytic pathway and topoisomerase I inhibition required further investigation. Finally, we have not yet investigated the expression levels of the multidrug efflux pumps encoded by *MDR1*. This could explain not only the resistance to ADCs, but also the reduced sensitivity to paclitaxel, which is a known substrate of this efflux pump [59].

5.3 Methodological considerations

5.3.1 Therapy studies in PDXCs *ex vivo*

There are several factors that may contribute to variations in the results obtained in PDXCs.

PDX tissue characteristics

The PDXCs might exhibit varied "behavior" due to the characteristics of the PDX tissue [74]. This became apparent when comparing the cultures of MAS98.12 and HBCx39. MAS98.12 is a softer tissue, which has shorter survival time, higher fraction of dead cells and limited growth *ex vivo* compared to HBCx39. This affected the choice of read-out methods for evaluating tissue sensitivity to drugs. Methods like live/dead staining of the cultured fragments was determined to be better suited for MAS98.12, while the Incucyte-based tracking of fragment size was the preferred method for HBCx39 [74]. The tumors used to develop the PDXCs may vary in size as well as level of necrosis. The tumor size and necrosis level might be associated with the tissue's viability and ability to grow *ex vivo*. As seen in Figure 16, the growth of the fragments in experiment 1 is much greater than in experiment 2. For experiment 1, big tumors (weighing approximately 1,2 g per tumor) were used, while for experiment 2, smaller tumors (weighing approximately 0,8 g per tumor) were used.

Furthermore, the tissue from different PDX models might respond differently to components in the culture medium or require certain factors for optimal growth. For example, Nutlin-3 is used to eliminate normal stromal cells from the culture. This approach is only suitable for tumors with lost or mutated *TP53*, which makes the cancer cells insensitive to Nutlin-3, resulting in the survival of only the malignant cells. *TP53* mutations are frequent in TNBCs [91], and this is the case also for MAS98.12 and HBCx39 tumors.

The presence of stromal cells in PDXCs

The removal of stromal cells from PDXCs might be a dilemma. On one hand, contamination of PDXCs with the host/mouse cells complicates the evaluation of treatment effect, especially when using methods like CTG. In this project, we attempted to make the PDXCs as "clean" as possible. On the other hand, the presence of stromal cells partially recapitualtes the tumor microenvironment, which might influence the PDXC's response to treatment [88]. Elimination of the stromal components limits the classes of drugs that can be tested on these models [73].

Heterogeneity of PDXCs

It has been reported previously that the tissue fragments of the PDXC platform might be heterogenous, e.g. express different levels of epithelial markers [74]. In this project, we demonstrate the heterogeneity with respect to the levels of the proliferation marker Ki67 (Figure 13). We observed Ki67+ and Ki67- areas within the fragments, indicating that only parts of the fragments are proliferative and these parts are distributed unevenly. The fragments with larger areas of proliferative tissue might respond to the treatment differently than the fragments with a smaller fraction of proliferative areas.

Culturing conditions

The culturing conditions for PDXCs might need to be optimized for specific tumor tissue. Medium components of the Reduced Clevers+ medium is carefully considered, and some of the components reported in [71] have been excluded from the experiments of this project. Also, the number of fragments per well is important for the optimal growth of the PDXCs. Furthermore, some of the read-out methods, like CTG, requires as equal as possible amount of tissue fragments to be applied to each well (discussed in chapter 5.3.2). The optimal number of fragments per well is around 50-60, but some variations might occur, as the fragments are counted manually by a microscope. Variations in amount of fragments per well might also occur when the fragment-Matrigel suspension droplets are seeded out.

5.3.2 Read-out methods

To be able to evaluate drug sensitivity in both PDXCs and cell line, several read-out methods were employed. The different methods provide information about different aspects of the drug-induced effects. Thereby, it is important to combine several methods when investigating the effect each drug has on the models.

Detection of treatment effects using cell cultures *in vitro*

In this thesis we employed paclitaxel-sensitive and -refractory MDA-MB468 cells to evaluate the effect of paclitaxel treatment by three commonly used methods: monitoring cell confluence by the Incucyte S3, and cell viability by two different assays (MTS and CTG). As seen in Figure 11, the same trend was seen when using Incucyte S3, MTS and CTG,

i.e. revealing a dose-dependent response and that the refractory cells were less sensitive to paclitaxel. This indicates that these three methods provide comparable information in such experiments, although MTS and CTG were more sensitive and detected a slightly higher effect than the Incucyte-based approach. The same was observed when measuring the treatment effects in PDXCs (as shown in Figures 16B and 17). Although the Incucyte-based approach is less sensitive, it has several advantages. First, it provides a possibility to track the effect over time, which is not possible with CTG. Second, the Incucyte approach is based on imaging and therefore allows for selection of cells/fragments that we want to track. This might be an advantage when working with heterogenous cultures like PDXCs, that consists of malignant tissue fragments of interest, but also contaminating stromal cells. The latter might be a challenge for methods like CTG, where it is not able to discriminate which cells that contribute to the measured signal.

Monitoring fragment area by the Incucyte S3

As reported in [74], evaluating response to drug treatment by measuring total fragment area with the Incucyte S3 organoid module, was unsuitable for the MAS98.12 PDXCs. The PDXCs from MAS98.12 have a high fraction of dead cells in the periphery of the fragments (both treated and untreated), as seen in Figure 12C. These dead cells contribute to the total area measured by the Incucyte S3, which impairs the correlation between fragment area and viability/growth [74]. As seen in Figure 12A and B, there are big variations in each measurement, resulting in non-smooth growth curves. This makes it difficult to interpret the results. Therefore, the responsiveness of MAS98.12 to drugs had to be assessed by alternative methods, like live/dead staining or CTG. For HBCx39, Incucyte S3-monitoring was suitable, as the untreated fragments usually contain few dead cells, and the measured increase in fragment area reflects the growth. For this model, there is generally a correlation between the drug response measured by Incucyte S3, CTG and live/dead staining.

Live/dead staining

In [74], it was determined that live/dead staining scores responsiveness of MAS98.12 tissue to anti-cancer drugs *ex vivo*. This method was also used for HBCx39-PDXCs, as an additional approach to validate the treatment effects registered by the Incucyte S3

and CTG. Additionally, it allows to visualize the treatment effects, i.e. whether the drug has cytostatic or cytotoxic influence.

Cell viability assay (CTG)

CellTiter-Glo® 3D Cell Viability Assay uses ATP-levels to measure the amount of viable cells in cultures. The assay depends on equal amount of tissue to be applied to each well [82] [92], otherwise big variations in the measured signal between parallel wells will occur. Thus, the SEM observed in Figure 17 might be due to variable amounts of tissue applied to parallel wells.

In conclusion, it is important to choose the most suitable method or combine several methods, in order to correctly detect the drug sensitivity of individual tumor tissue.

5.3.3 Immunofluorescent staining

When performing immunofluorescent staining on 3D structures like tissue fragments or organoids, there are certain factors that need to be considered. In the case of the PDXCs, the fragment sizes are quite variable, meaning that the larger fragments might not be all the way permeabilized. When the permeabilization time is too short, the antibodies are not able to reach the core of the fragments, and it will look like there is no expression of the antigen in that region. On the contrary, the smaller fragments might seem to have a higher expression of the antigen. Therefore, when comparing fragments from different groups, one should try to look for two fragments of approximately the same size. To be able to quantify the difference in protein expression, more quantitative methods should be used, e.g. western blotting or flow cytometry. Unfortunately, this was not performed in this project due to time limitations. However, the advantage of IF is that it allows to investigate whether the protein expression is homogenous, both within the fragment and between several fragments.

In order to optimize the immunofluorescent staining procedure, and for the cells to be more permeabilized, the permeabilization time was increased from 30 minutes to 1 hour using 0,2% Triton. This was done because of the large size of some of the fragments. When the permeabilization time was increased, also the innermost cells were stained. High scattering of thick tissues can be a challenge for the imaging of 3D structures

because of the differences in refractive index of the different cellular components. Because of this, the fructose-glycerol clearing solution was added to optimize the imaging of the 3D structures. Tissue clearing limits the decline in fluorescence in the z-direction, making it possible to image the whole organoid also in the z-direction. In addition, the organoids can be stored long term at -20℃ when covered in clearing solution [76].

5.4 Future perspectives

Regarding the multidrug resistance of HBCx39ER, it would be interesting to investigate whether one or several of the endocytic pathway members may be involved in the development of resistance. The RAB5 immunofluorescence experiment should be performed again, under optimized conditions. In future experiments, RAB5 should be costained with an early endosome marker (e.g. EEA1), to be able to confirm that the RAB5 staining is localized on the early endosomes. To be able to compare the expression levels of the sensitive and resistant sublines of HBCx39, HBCx39ER should also be stained for RAB5.

Additionally, the expression level of multidrug transporters should be investigated. The P-glycoprotein pump (encoded by the *MDR1* gene) is associated with multidrug resistance in BC. The protein might cause resistance independently, or the resistance might be due to several resistance mechanisms acting in combination [93]. The expression level of these could be investigated further, comparing the drug-sensitive and -resistant sublines of HBCx39, using e.g. flow cytometry [94].

As described in this thesis, BC cells may develop resistance to ADCs when exposed to treatment over time. Therefore, it might be useful to study the effects of ADC in combination with other anticancer therapies [95]. It would be interesting to explore the use of combination therapy on the drug resistant tumor tissue, using the PDXC platform. During recent years, ADC-based combination therapies for the treatment of several cancer types have been actively studied. In BC, ADCs have been reported to have enhanced antitumor effect when combined with e.g. targeted therapy [96] and chemotherapy [97], [98]. Based on these reports, it would be interesting to test Enhertu and Trodelvy in combination with other anti-cancer therapies, using the TNBC PDXC models.

Further down the line, we are hoping that this platform can be used in the personalized treatment of BC patients, deciding which treatment options are suitable for the individual patient and to characterize possible resistance.

Conclusion

In conclusion, PDXC is a useful platform to predict drug sensitivity and to investigate resistance mechanisms *ex vivo*. Specifically, we have demonstrated that PDXCs from Enhertu-sensitive and -resistant PDXs show sensitivity and resistance to Enhertu, respectively, indicating that the *ex vivo* effects recapitulate the results seen *in vivo*.

Furthermore, we have shown that PDXCs from Enhertu-resistant PDXs are less sensitive to Trodelvy and paclitaxel, predicting that those PDXs should be less sensitive to the indicated drugs also *in vivo*, which was validated later by other members of the group. In addition, this data indicates that Enhertu-resistant tumors utilize resistance mechanisms that are not restricted to Enhertu, i.e. display multidrug resistance.

Several possible resistance mechanisms were investigated without revealing the exact mechanism developed by the HBCx39ER PDX. Specifically, we detected equal expression of HER2 and Trop-2, and equal sensitivity to the topoisomerase I inhibitor, irinotecan, in the Enhertu-sensitive and -resistant PDXCs. This suggests that neither receptor-binding of ADCs nor payload target are the reasons for the Enhertu-resistance.

References

[1] Lauren Pecorino. *Molecular Biology of Cancer*. 4th ed. Oxford University Press, 2016. ISBN: 978-0-19-871734-8.

[2] Bert Vogelstein et al. 'Cancer genome landscapes'. In: *science* 339.6127 (2013), pp. 1546–1558.

[3] Ashley Matusz-Fisher and Antoinette R Tan. 'Combination of HER2-targeted agents with immune checkpoint inhibitors in the treatment of HER2-positive breast cancer'. In: *Expert Opinion on Biological Therapy* 22.3 (2022), pp. 385–395.

[4] Carolina Gutierrez and Rachel Schiff. 'HER2: biology, detection, and clinical implications'. In: *Archives of pathology & laboratory medicine* 135.1 (2011), pp. 55–62.

[5] Gaoyang Zhu et al. 'Mutant p53 in cancer progression and targeted therapies'. In: *Frontiers in oncology* 10 (2020), p. 595187.

[6] Eva YHP Lee and William J Muller. 'Oncogenes and tumor suppressor genes'. In: *Cold Spring Harbor perspectives in biology* 2.10 (2010), a003236.

[7] Ellen L Goode, Cornelia M Ulrich and John D Potter. 'Polymorphisms in DNA repair genes and associations with cancer risk'. In: *Cancer epidemiology biomarkers & prevention* 11.12 (2002), pp. 1513–1530.

[8] Christine L Chaffer and Robert A Weinberg. 'A perspective on cancer cell metastasis'. In: *science* 331.6024 (2011), pp. 1559–1564.

[9] Douglas Hanahan and Robert A Weinberg. 'The hallmarks of cancer'. In: *cell* 100.1 (2000), pp. 57–70.

[10] Scott Valastyan and Robert A Weinberg. 'Tumor metastasis: molecular insights and evolving paradigms'. In: *Cell* 147.2 (2011), pp. 275–292.

[11] Robert A. Weinberg. *The Biology of Cancer*. 2nd ed. Garland Science, 2014. ISBN: 978-0-8153-4220-5.

[12] Sarah Heerboth et al. 'EMT and tumor metastasis'. In: *Clinical and translational medicine* 4.1 (2015), pp. 1–13.

[13] Anushka Dongre and Robert A Weinberg. 'New insights into the mechanisms of epithelial–mesenchymal transition and implications for cancer'. In: *Nature reviews Molecular cell biology* 20.2 (2019), pp. 69–84.

[14] Kreftregisteret. *Brystkreft*. URL: https://www.kreftregisteret.no/Temasider/kreftformer/Brystkreft/. (Accessed August 2023).

[15] Carol E DeSantis et al. 'Cancer treatment and survivorship statistics, 2014'. In: *CA: a cancer journal for clinicians* 64.4 (2014), pp. 252–271.

[16] Yixiao Feng et al. 'Breast cancer development and progression: Risk factors, cancer stem cells, signaling pathways, genomics, and molecular pathogenesis'. In: *Genes & diseases* 5.2 (2018), pp. 77–106.

[17] Madhur Gupta and Neeru Goyal. 'Applied anatomy of breast cancer'. In: *Breast Cancer: Comprehensive Management*. Springer, 2022, pp. 23–35.

[18] Xin Lu and Yibin Kang. 'Organotropism of breast cancer metastasis'. In: *Journal of mammary gland biology and neoplasia* 12 (2007), pp. 153–162.

[19] Erasmo Orrantia-Borunda et al. 'Subtypes of breast cancer'. In: *Breast Cancer [Internet]* (2022).

[20] Aron Goldhirsch et al. 'Personalizing the treatment of women with early breast cancer: highlights of the St Gallen International Expert Consensus on the Primary Therapy of Early Breast Cancer 2013'. In: *Annals of oncology* 24.9 (2013), pp. 2206–2223.

[21] Elena Dìaz-Rodrìguez et al. 'Novel ADCs and strategies to overcome resistance to anti-HER2 ADCs'. In: *Cancers* 14.1 (2021), p. 154.

[22] Valeria Ossovskaya et al. 'Exploring molecular pathways of triple-negative breast cancer'. In: *Genes & cancer* 2.9 (2011), pp. 870–879.

[23] Lei Zhang et al. 'Identifying ultrasound and clinical features of breast cancer molecular subtypes by ensemble decision'. In: *Scientific reports* 5.1 (2015), p. 11085.

[24] Francesca Rastelli and Sergio Crispino. 'Factors predictive of response to hormone therapy in breast cancer'. In: *Tumori Journal* 94.3 (2008), pp. 370–383.

[25] Jens Hasskarl. 'Everolimus'. In: *Small molecules in oncology* (2018), pp. 101–123.

[26] In Hae Park et al. 'Phase I/II clinical trial of everolimus combined with gemcitabine/cisplatin for metastatic triple-negative breast cancer'. In: *Journal of Cancer* 9.7 (2018), p. 1145.

[27] Denise A Yardley et al. 'Everolimus plus exemestane in postmenopausal patients with HR+ breast cancer: BOLERO-2 final progression-free survival analysis'. In: *Advances in therapy* 30 (2013), pp. 870–884.

[28] Clifford A Hudis. 'Trastuzumab—mechanism of action and use in clinical practice'. In: *New England journal of medicine* 357.1 (2007), pp. 39–51.

[29] Ilana Schlam and Sandra M Swain. 'HER2-positive breast cancer and tyrosine kinase inhibitors: the time is now'. In: *NPJ breast cancer* 7.1 (2021), p. 56.

[30] Pankaj Kumar and Rupali Aggarwal. 'An overview of triple-negative breast cancer'. In: *Archives of gynecology and obstetrics* 293 (2016), pp. 247–269.

[31] Peter Nygren. 'What is cancer chemotherapy?' In: *Acta Oncologica* 40.2-3 (2001), pp. 166–174.

[32] GN Hortobagyi. 'Anthracyclines in the treatment of cancer: an overview'. In: *Drugs* 54 (1997), pp. 1–7.

[33] Ashkan Emadi, Richard J Jones and Robert A Brodsky. 'Cyclophosphamide and cancer: golden anniversary'. In: *Nature reviews Clinical oncology* 6.11 (2009), pp. 638–647.

[34] Norsk Bryst Cancer Gruppe (NBCG). *Retningslinjer*. URL: https://nbcg.no/retningslinjer/. (Accessed September 2023).

[35] Beth A Weaver. 'How Taxol/paclitaxel kills cancer cells'. In: *Molecular biology of the cell* 25.18 (2014), pp. 2677–2681.

[36] Kamal S Saini et al. 'Antibody-drug conjugates, immune-checkpoint inhibitors, and their combination in breast cancer therapeutics'. In: *Expert Opinion on Biological Therapy* 21.7 (2021), pp. 945–962.

[37] Alice Indini, Erika Rijavec and Francesco Grossi. 'Trastuzumab deruxtecan: changing the destiny of HER2 expressing solid tumors'. In: *International journal of molecular sciences* 22.9 (2021), p. 4774.

[38] Chiara Corti et al. 'Antibody–drug conjugates for the treatment of breast cancer'. In: *Cancers* 13.12 (2021), p. 2898.

[39] Beslutningsforum. *Protokoll – (til godkjenning)*. URL: https://nyemetoder.no/Documents/Beslutninger/Beslutningsforum%2025092023_Protokoll.pdf. (Accessed September 2023).

[40] Anupama Samantasinghar et al. 'A comprehensive review of key factors affecting the efficacy of antibody drug conjugate'. In: *Biomedicine & Pharmacotherapy* 161 (2023), p. 114408.

[41] Jessica R McCombs and Shawn C Owen. 'Antibody drug conjugates: design and selection of linker, payload and conjugation chemistry'. In: *The AAPS journal* 17 (2015), pp. 339–351.

[42] Emin Oroudjev et al. 'Maytansinoid-antibody conjugates induce mitotic arrest by suppressing microtubule dynamic instability'. In: *Molecular cancer therapeutics* 9.10 (2010), pp. 2700–2713.

[43] Michinori Akaiwa, Julien Dugal-Tessier and Brian A Mendelsohn. 'Antibody–drug conjugate payloads; study of auristatin derivatives'. In: *Chemical and Pharmaceutical Bulletin* 68.3 (2020), pp. 201–211.

[44] Nicole M Baker, Rakhi Rajan and Alfonso Mondragón. 'Structural studies of type I topoisomerases'. In: *Nucleic acids research* 37.3 (2009), pp. 693–701.

[45] Yves Pommier. 'Topoisomerase I inhibitors: camptothecins and beyond'. In: *Nature Reviews Cancer* 6.10 (2006), pp. 789–802.

[46] Ying Fu and Mitchell Ho. 'DNA damaging agent-based antibody-drug conjugates for cancer therapy'. In: *Antibody therapeutics* 1.2 (2018), pp. 43–53.

[47] David M Goldenberg et al. 'Trop-2 is a novel target for solid cancer therapy with sacituzumab govitecan (IMMU-132), an antibody-drug conjugate (ADC)'. In: *Oncotarget* 6.26 (2015), p. 22496.

[48] Jonathan D Bargh et al. 'Cleavable linkers in antibody–drug conjugates'. In: *Chemical Society Reviews* 48.16 (2019), pp. 4361–4374.

[49] Federica Giugliano et al. 'Bystander effect of antibody–drug conjugates: fact or fiction?' In: *Current oncology reports* 24.7 (2022), pp. 809–817.

[50] Alexander H Staudacher and Michael P Brown. 'Antibody drug conjugates and bystander killing: is antigen-dependent internalisation required?' In: *British journal of cancer* 117.12 (2017), pp. 1736–1742.

[51] Ravi VJ Chari, Michael L Miller and Wayne C Widdison. 'Antibody–drug conjugates: an emerging concept in cancer therapy'. In: *Angewandte Chemie International Edition* 53.15 (2014), pp. 3796–3827.

[52] Olav Engebraaten et al. 'RAB5A expression is a predictive biomarker for trastuzumab emtansine in breast cancer'. In: *Nature communications* 12.1 (2021), p. 6427.

[53] Marino Zerial and Heidi McBride. 'Rab proteins as membrane organizers'. In: *Nature reviews Molecular cell biology* 2.2 (2001), pp. 107–117.

[54] Ellen Adams et al. 'Sacituzumab govitecan and trastuzumab deruxtecan: two new antibody–drug conjugates in the breast cancer treatment landscape'. In: *ESMO open* 6.4 (2021), p. 100204.

[55] Aditya Bardia et al. 'Sacituzumab govitecan-hziy in refractory metastatic triple-negative breast cancer'. In: *New England Journal of Medicine* 380.8 (2019), pp. 741–751.

[56] Heinz Hammerlindl and Helmut Schaider. 'Tumor cell-intrinsic phenotypic plasticity facilitates adaptive cellular reprogramming driving acquired drug resistance'. In: *Journal of cell communication and signaling* 12 (2018), pp. 133–141.

[57] Shunji Takahashi et al. 'Gene therapy for breast cancer.—Review of clinical gene therapy trials for breast cancer and MDR1 gene therapy trial in Cancer Institute Hospital'. In: *Breast Cancer* 13 (2006), pp. 8–15.

[58] Karin Hientz et al. 'The role of p53 in cancer drug resistance and targeted chemotherapy'. In: *Oncotarget* 8.5 (2017), p. 8921.

[59] Elena Galletti et al. 'Paclitaxel and docetaxel resistance: molecular mechanisms and development of new generation taxanes'. In: *ChemMedChem: Chemistry Enabling Drug Discovery* 2.7 (2007), pp. 920–942.

[60] Vlasta Němcová-Fürstová et al. ‘Characterization of acquired paclitaxel resistance of breast cancer cells and involvement of ABC transporters’. In: *Toxicology and applied pharmacology* 310 (2016), pp. 215–228.

[61] Michaela J Higgins, José Baselga et al. ‘Targeted therapies for breast cancer’. In: *The Journal of clinical investigation* 121.10 (2011), pp. 3797–3803.

[62] Maurizio Scaltriti et al. ‘Expression of p95HER2, a truncated form of the HER2 receptor, and response to anti-HER2 therapies in breast cancer’. In: *Journal of the National Cancer Institute* 99.8 (2007), pp. 628–638.

[63] Guangmin Li et al. ‘Mechanisms of acquired resistance to trastuzumab emtansine in breast cancer cells’. In: *Molecular cancer therapeutics* 17.7 (2018), pp. 1441–1453.

[64] Frank Loganzo et al. ‘Tumor cells chronically treated with a trastuzumab–maytansinoid antibody–drug conjugate develop varied resistance mechanisms but respond to alternate treatments’. In: *Molecular cancer therapeutics* 14.4 (2015), pp. 952–963.

[65] FB De Abreu et al. ‘Personalized therapy for breast cancer’. In: *Clinical genetics* 86.1 (2014), pp. 62–67.

[66] Christophe Massard et al. ‘High-throughput genomics and clinical outcome in hard-to-treat advanced cancers: results of the MOSCATO 01 trial’. In: *Cancer discovery* 7.6 (2017), pp. 586–595.

[67] Lacey E Dobrolecki et al. ‘Patient-derived xenograft (PDX) models in basic and translational breast cancer research’. In: *Cancer and Metastasis Reviews* 35 (2016), pp. 547–573.

[68] Anna Bergamaschi et al. ‘Molecular profiling and characterization of luminal-like and basal-like in vivo breast cancer xenograft models’. In: *Molecular oncology* 3.5-6 (2009), pp. 469–482.

[69] Annette T Byrne et al. ‘Interrogating open issues in cancer precision medicine with patient-derived xenografts’. In: *Nature Reviews Cancer* 17.4 (2017), pp. 254–268.

[70] Alejandra Bruna et al. ‘A biobank of breast cancer explants with preserved intra-tumor heterogeneity to screen anticancer compounds’. In: *Cell* 167.1 (2016), pp. 260–274.

[71] Norman Sachs et al. 'A living biobank of breast cancer organoids captures disease heterogeneity'. In: *Cell* 172.1 (2018), pp. 373–386.

[72] Johanna F Dekkers et al. 'Long-term culture, genetic manipulation and xenotransplantation of human normal and breast cancer organoids'. In: *Nature protocols* 16.4 (2021), pp. 1936–1965.

[73] Katrin P Guillen et al. 'A human breast cancer-derived xenograft and organoid platform for drug discovery and precision oncology'. In: *Nature cancer* 3.2 (2022), pp. 232–250.

[74] Solveig Pettersen et al. 'Breast cancer patient-derived explant cultures recapitulate in vivo drug responses'. In: *Frontiers in Oncology* 13 (2023), p. 1040665.

[75] ATCC. *MDA-MB-468*. URL: https://www.atcc.org/products/htb-132. (Accessed January 2023.

[76] Johanna F Dekkers et al. 'High-resolution 3D imaging of fixed and cleared organoids'. In: *Nature protocols* 14.6 (2019), pp. 1756–1771.

[77] Promega. *CellTiter 96® AQueous One Solution Cell Proliferation Assay (MTS)*. URL: https://no.promega.com/products/cell-health-assays/cell-viability-and-cytotoxicity-assays/celltiter-96-aqueous-one-solution-cell-proliferation-assay-_mts_/?catNum=G3582#protocols. (Accessed September 2023).

[78] Promega. *CellTiter-Glo® 2.0 Assay*. URL: https://www.promega.com/-/media/files/resources/protocols/technical-manuals/101/celltiterglo-2-0-assay-protocol.pdf?la=en. (Accessed November 2023).

[79] Fei Duan et al. 'Area under the curve as a tool to measure kinetics of tumor growth in experimental animals'. In: *Journal of immunological methods* 382.1-2 (2012), pp. 224–228.

[80] ThermoFisher Scientific. *Propidium Iodide*. URL: https://www.thermofisher.com/no/en/home/life-science/cell-analysis/fluorophores/propidium-iodide.html. (Accessed September 2023).

[81] PromoKine. *Calcein AM*. URL: https://www.promocell.com/app/uploads/2018/01/PK-CA707-80011.pdf. (Accessed September 2023).

[82] Promega. *CellTiter-Glo® 3D Cell Viability Assay*. URL: https://no.promega.com/products/cell-health-assays/cell-viability-and-cytotoxicity-assays/celltiter-glo-3d-cell-viability-assay/?catNum=G9681#protocols. (Accessed September 2023).

[83] Haatisha Jandu et al. 'Molecular characterization of irinotecan (SN-38) resistant human breast cancer cell lines'. In: *BMC cancer* 16.1 (2016), pp. 1–13.

[84] Thermofisher. *pan Cytokeratin (pan CK) Monoclonal Antibody (AE1+AE3), TrueMAB™*. URL: https://www.thermofisher.com/antibody/product/pan-Cytokeratin-pan-CK-Antibody-clone-AE1-AE3-Monoclonal/CF190321. (Accessed May 2023).

[85] Rebecca Dent et al. 'Triple-negative breast cancer: clinical features and patterns of recurrence'. In: *Clinical cancer research* 13.15 (2007), pp. 4429–4434.

[86] Shanu Modi et al. 'Trastuzumab deruxtecan in previously treated HER2-low advanced breast cancer'. In: *New England Journal of Medicine* 387.1 (2022), pp. 9–20.

[87] Julia E McGuinness and Kevin Kalinsky. 'Antibody-drug conjugates in metastatic triple negative breast cancer: A spotlight on sacituzumab govitecan, ladiratuzumab vedotin, and trastuzumab deruxtecan'. In: *Expert Opinion on Biological Therapy* 21.7 (2021), pp. 903–913.

[88] Ian R Powley et al. 'Patient-derived explants (PDEs) as a powerful preclinical platform for anti-cancer drug and biomarker discovery'. In: *British journal of cancer* 122.6 (2020), pp. 735–744.

[89] Esmaeil Dorraji et al. 'Development of a High-Affinity Antibody against the Tumor-Specific and Hyperactive 611-p95HER2 Isoform'. In: *Cancers* 14.19 (2022), p. 4859.

[90] Céline Gongora et al. 'New Topoisomerase I mutations are associated with resistance to camptothecin'. In: *Molecular cancer* 10 (2011), pp. 1–13.

[91] Zuzana Sporikova et al. 'Genetic markers in triple-negative breast cancer'. In: *Clinical breast cancer* 18.5 (2018), pp. 841–850.

[92] Rita Hannah et al. 'CellTiter-Glo™ Luminescent cell viability assay: a sensitive and rapid method for determining cell viability'. In: *Promega Cell Notes* 2 (2001), pp. 11–13.

[93] Bruce J Trock, Fabio Leonessa and Robert Clarke. 'Multidrug resistance in breast cancer: a meta-analysis of MDR1/gp170 expression and its possible functional significance'. In: *Journal of the National Cancer Institute* 89.13 (1997), pp. 917–931.

[94] Eugene Mechetner et al. 'Levels of multidrug resistance (MDR1) P-glycoprotein expression by human breast cancer correlate with in vitro resistance to taxol and doxorubicin.' In: *Clinical cancer research: an official journal of the American Association for Cancer Research* 4.2 (1998), pp. 389–398.

[95] Jesús Fuentes-Antrás et al. 'Antibody–drug conjugates: In search of partners of choice'. In: *Trends in Cancer* (2023).

[96] Virginia F Borges et al. 'Tucatinib combined with ado-trastuzumab emtansine in advanced ERBB2/HER2-positive metastatic breast cancer: a phase 1b clinical trial'. In: *JAMA oncology* 4.9 (2018), pp. 1214–1220.

[97] Ian E Krop et al. 'Phase 1b/2a study of trastuzumab emtansine (T-DM1), paclitaxel, and pertuzumab in HER2-positive metastatic breast cancer'. In: *Breast Cancer Research* 18 (2016), pp. 1–10.

[98] M Martin et al. 'Trastuzumab emtansine (T-DM1) plus docetaxel with or without pertuzumab in patients with HER2-positive locally advanced or metastatic breast cancer: results from a phase Ib/IIa study'. In: *Annals of Oncology* 27.7 (2016), pp. 1249–1256.

Appendix

7.1 Materials

Table 7.1: Drugs used in the drug sensitivity assessment screen.

Drug	**Supplier**	**Catalogue number**
Everolimus	LC laboratories	E-4040
Paclitaxel	Fresenius Kabi	L01C D01
Trodelvy	Gilead Sciences Nordic	L01F X17
Enhertu	Daiicki Sankyo Nordic ApS	L01F D04
Irinotecan	Fresenius Kabi	L01C E02